GRANT/ LEWIS

IN- 35679

ENERGY LABORATORY

MASSACHUSETTS INSTITUTE OF TECHNOLOGY

p-85

FINAL REPORT

PROCESSING OF LASER FORMED SiC POWDER

Principal Investigators:

J. S. Haggerty

H. K. Bowen

Grant: NAG3-312

Effective Dates: July 30, 1982 - Dec. 31, 1985

Technical Officer: Dr. Sunil Dutta

Sponsor: NASA-Lewis Research Center

Contractor: Energy Laboratory
Massachusetts Institute of Technology
Cambridge, Massachusetts 02139

ACKNOWLEDGMENTS

Because this program has a broader scope than could be addressed in significant depth with its nominally 1 man-year per year level of effort, this report draws on results from our overall powder processing program that align with this program's research objectives. Many have made individual contributions that either have or will be the subjects of technical publications. Specifically, Mr. J. Flint and Dr. K. Sawano conducted synthesis research that led to larger diameter, ideal SiC powders; dispersion research topics were carried out by Mr. M. Okuyama, Mr. M. Aoki and Mr. G. Garvey with Prof. T. Ring's supervision; Mr. G. Garvey conduted the part fabrication research; drying studies were done by Mr. D. Castro with Prof. Ring's supervision; consolidation experiments were done by Mr. Aoki and Mr. Okuyama; mechanical property measurements were made at the University of Massachusetts under Prof. J. Ritter's supervision. Citations to presentations and/or publications resulting from these individual contributions are references 2, 11, 12, 31, 34, 35, 36 and 50. Finally metallographic sections of sintered samples were prepared by NASA-Lewis.

All contributions are gratefully acknowledged.

TABLE OF CONTENTS

LIST OF FIGURES

LIST OF FIGURES (continued)

LIST OF FIGURES (continued)

LIST OF TABLES

ABSTRACT

Processing research was undertaken to demonstrate that superior SiC characteristics could be achieved through the use of ideal constituent powders and careful post-synthesis processing steps.

Initial research developed means to produce ~1000 Å uniform diameter, nonagglomerated, spherical, high purity SiC powders. Accomplishing this goal required major revision of the particle formation and growth model from one based on classical nucleation and growth to one based on collision and coalescence of Si particles followed by their carburization. Dispersions based on pure organic solvents as well as steric stabilization were investigated. Although stable dispersions were formed by both, subsequent part fabrication emphasized the pure solvents because we anticipated fewer problems with drying and residuals on the high purity particles. Test parts were made by the colloidal pressing technique; both liquid filtration and consolidation (rearrangement) stages were modeled. Green densities corresponding to a random close packed structure (~63%) were achieved; this highly perfect structure has a high, uniform coordination number (>11) approaching the quality of an ordered structure without introducing domain boundary defects. After drying, parts were densified at temperatures ranging from 1800 to 2100°C. Optimum densification temperatures will probably be in the 1900-2000°C range based on these preliminary results which showed that 2050°C samples had experienced substantial grain growth. Although overfired, the 2050°C samples exhibited excellent mechanical properties. Biaxial tensile strengths up to 714 MPa and Vickers hardness values of 2430 kg/mm^2 were both more typical of hot pressed than sintered SiC. Both result from the absence of large defects and the confinement of residual porosity (<2.5%) to small diameter, uniformly distributed pores.

This research program accomplished all of its major objectives. Superior microstructures and properties were attained by using powders having ideal characteristics and special post-synthesis processing procedures.

I. INTRODUCTION

We at M.I.T. have approached the historic subject of ceramic property-processing interactions from a new prospective. We hypothesized and are now demonstrating through government and industrially sponsored research that powder processes and resulting properties of ceramic bodies can be dramatically improved by using powders having unconventional characteristics. The principal new feature is requiring that the powders have a uniform particle size so that the flaw characteristics, density uniformity, and coordination number in the green bodies all can be improved simultaneously at the expense of a small decrease in green density level. A laser heated gas phase synthesis process has been developed to produce nonoxide ceramic powders having the required characteristics.

Defects in ceramic bodies are usually attributable to some specific event in the processing history of a component,[1] extending from powder synthesis through all the handling steps to the final consolidation into a densified part. There are many causes for strength limiting defects and their elimination continues to be the subject of processing research and component development programs. Our approach to resolving this problem requires that constituent powders satisfy rigid criteria.[2] With highly specific powders and the correct handling procedures, it is possible to cause the individual particles to arrange in a close packed structure as shown in Figure 1 or more practically in a random close packed structure[3] which has many of the same attributes. Bodies having this unusual internal structure will exhibit precisely definable, uniform shrinkage to theoretical density with low firing temperatures and short firing times. These densification cycles should virtually eliminate grain growth. Also, the

characteristic size of remaining flaws should be approximately that of the particles since individual particle vacancies are the largest probable defect.

Our research has demonstrated that the powders must have the following ideal characteristics: (1) the powder must have a small particle size, typically less than 0.5 μm; (2) the powder must be free of agglomerates; (3) the particle diameters must have a narrow range of sizes; (4) the morphology of the particles must be equiaxed, tending toward spherical shapes; (5) the powders must have highly controlled purity with respect to contaminants and to multiple polymorphic phases. Either with the ordered structures shown in Figure 1 or random close packed structures, a powder exhibiting these ideal characteristics should be sinterable to theoretical density without resorting to pressure or additives and should permit the final grain structure to be highly controllable.

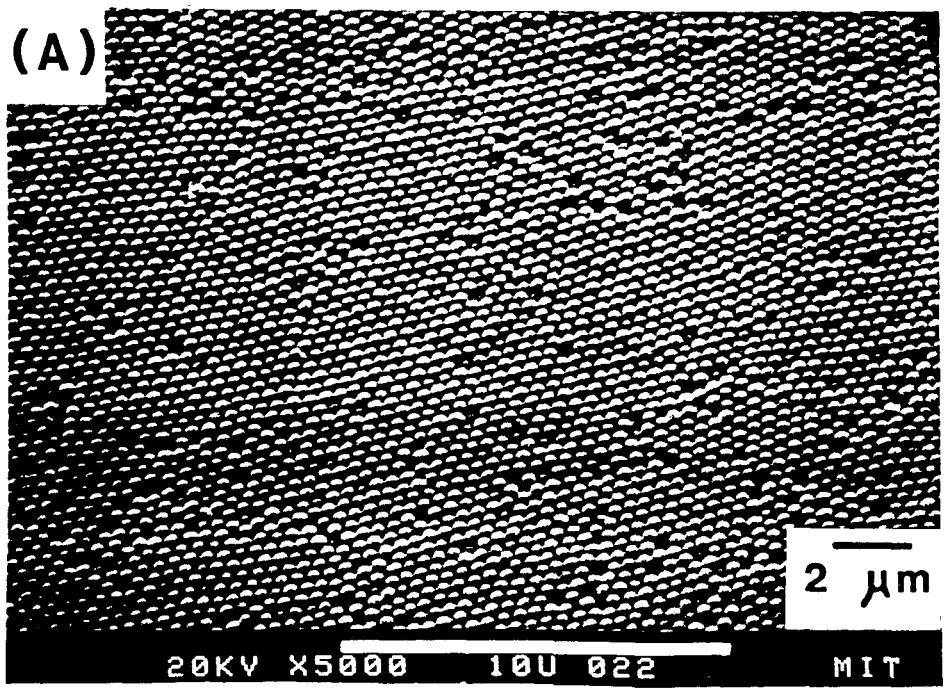

Figure 1. Ordered packing of monodispersed 0.2 μm diameter TiO_2 spheres. (Barringer Ref. 24)

Because existing powder synthesis techniques could not produce powders with these requisite characteristics, we developed a laser heated gas phase synthesis process. The laser driven gas phase reaction process offers many advantages. It is a clean process because no potentially contaminating surfaces are heated. The reaction zone is precisely defined, consisting of the volume enclosed by the reactant gas stream and the laser beam. The ability to maintain steep temperature gradients in the effective thermal environment, and thus a well defined reaction zone, allows precise control of the nucleation rate, the growth rate and exposure times, permitting the nucleation and growth of very fine uniformly sized particles. Virtually 100% of the reactants are consumed and the processing energy is projeted to be only 2-3 kWhr/kg of powder.

Before starting this program, our research had emphasized synthesis of Si and Si_3N_4.[4-7] The feasibility of synthesizing SiC had been demonstrated[8] but process conditions had to be identified that would result in approximately 1000 Å diameter agglomerate-free particles.

II. APPROACH

This research program had three tasks; each to be carried out sequentially during the course of the proposed three year program. In the first we were to define process conditions leading to suitable SiC powders, in the second we were to find means to disperse the powders, and in the third we were to shape and consolidate powders.

The first year's objective was to grow nominally 1000 Å diameter SiC powders having all requisite characteristics. The most important characteristics are freedom from agglomerates and narrow size distribution.

Other important characteristics are stoichiometry, crystallinity (amorphous or specific crystalline phase), purity and shape. This task was continued into the second and third years.

The primary objective for the second year was to find means of dispersing the SiC powders which will insure that all particles are reliably separated. The dispersing liquid must not contaminate the powders, must be completely removable and should be reasonably free of both toxicity and combustion problems. We had previously investigated the dispersion of Si powder after capture in the filter assembly.[9] These results and the results of more recent calculations provided the initial basis for selecting dispersants for SiC.

Year three's research introduced shaping and consolidation issues in conjunction with continued synthesis and dispersion research topics. Introduction of subsequent processing steps required reexamination and reoptimization of synthesis and dispersion processing steps. SiC parts were made by centrifugal casting and by colloidal pressing techniques. Densification was limited to pressureless sintering with B as a sintering aid. Resulting parts were characterized microstructurally and mechanically.

III. SiC POWDER SYNTHESIS

A. Description of the Synthesis Process

The powder synthesis process[4-7] employs an optical energy source to transfer the energy required to initiate and sustain a chemical reaction in the gas phase. In this process, the gas molecules are "self-heated" throughout the gas volume, a process that is distinct from conventional ones where heat is transmitted from a source to the gas molecules by a

combination of conduction, convection and radiative processes. The advantages of this means of heating are freedom from contamination, absence of surfaces that act as heterogeneous nucleation sites, and unusually uniform and precise process control. These attributes permit synthesis of powders with characteristics that are ideal for making ceramic bodies.

In the experimental apparatus, Figure 2, the laser beam enters the reaction chamber through a KCl window and is either arrested with a water cooled copper block or exits through a second KCl window. Power intensities range from 270-1020 watts/cm^2 for the unfocused beam, and up to 10^5 watts/cm^2 near the focal point of a 13 cm lens. The reactant gases (SiH_4 for Si, NH_3-SiH_4 for Si_3N_4, and either CH_4-SiH_4 or C_2H_4-SiH_4 for SiC) enter

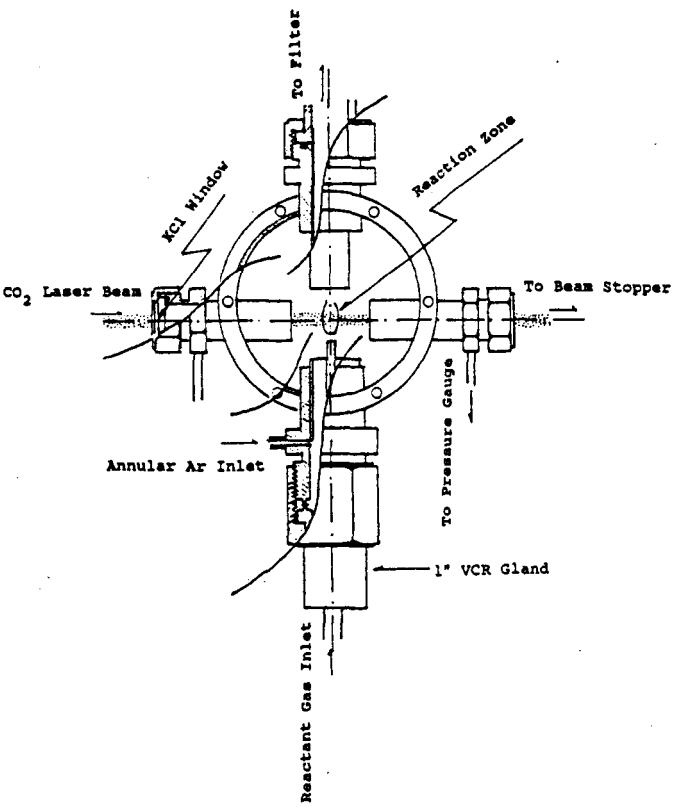

Figure 2. Schematic of powder synthesis cell.

the cell orthogonal to the laser beam through a 1.5 mm stainless steel nozzle 2-3 mm below the laser beam. A coaxial argon stream is used to suppress the expansion of the product stream with entrained particles, so these particles can be collected in a microfiber filter. Argon gas is directed across the KCl window to prevent powder collection there and possible breakage. A typical Si_3N_4 reaction flame is shown schematically in Figure 3. The reactant gases employed are electronic grade SiH_4, NH_3, CH_4 and C_2H_4. Prepurified argon is used as the inert buffer gas. The Ar gas train includes a Ti oxygen getter that typically achieves < 1 ppm O_2. Reaction cell pressures, ranging from 0.08 to 2.0 atm, are maintained by a throttling valve in series between the filter and the vacuum pump. Sintering enhancing additives are introduced in the reactant gas stream; e.g. boron as B_2H_6.

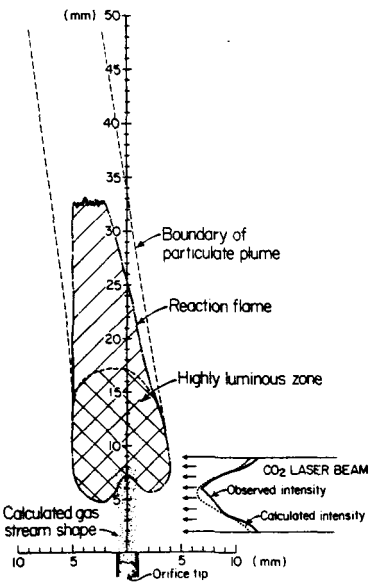

Figure 3. Physical characteristics of a typical laser induced Si_3N_4 reaction. The reaction flame is shown relative to the gas nozzle and laser beam positions.

The powders produced in the reaction zone are carried into the collection filter by the product and argon gases. With recent modifications, virtually all of the powder is transported to the filter. Based on mass balance, the laser induced reaction typically converts 85 - 100% of the reactants to products. After termination of a synthesis experiment, the collected powders are sealed in the microfiber filter under a positive argon pressure; the filter assembly is then transferred into a glove box through a vacuum antechamber. All post-production handling is performed in an argon environment maintained at less than 10 ppm each of O_2 and H_2O. None of these powders oxidize pyrophorically on exposure to air.

Most process variables were manipulated systematically[4-7] to determine their effect on particle characteristics. The variables that have a direct effect on the formation and growth kinetics include reaction temperature, heating rate, partial pressure of reactants, total pressure and dilution by inert gases. Most of these variables were manipulated to demonstrate their effects on SiC powder characteristics. We examined the following powder characteristics: size, size distribution, shape, stoichiometry, chemical impurities, and crystallinity.

The identification of the particle formation process was the primary and the essential result of these synthesis experiments. Our original synthesis model was basically classical nucleation and growth.[10] This model had some success, especially in describing low temperature, low pressure reactions that produced small particles. However, this model had several problems in describing process conditions leading to larger Si particles

and, in particular, with respect to SiC synthesis from a SiH_4 reactant. Our current SiC synthesis model[11,12] has a Si formation and growth step followed by a carburization step. The Si particle formation and growth occurs by collision and coalescence.

Based on an improved understanding of the operative mechanisms, it was possible to increase the mean SiC particle diameter from nominally 100Å to over 900Å while retaining complete dispersibility. Partially dispersible SiC powders with diameters up to approximately 1500Å were produced.

B. Particle Formation Model

A successful model for the formation of silicon particles by the laser process must explain how the process variables determine the final size of the particles, the particle size distribution, and the final morphology distribution of the particles. The last point is crucial since of the three types of silicon particles, (I: 50-200 Å agglomerated spheres, II: 200-1000 Å linear aggregates, and III: 500-5000 Å isolated spheres) it is the Type III powders that are needed for ceramic processing. We found that the type III Si particles must form before carburization commenced to achieve the desired SiC powder characteristics.

1. Coalescence Model

a. Mechanism

The basis of the coalescence model is that silane rapidly decomposes to either silicon or di-silicon particles which make larger and larger particles through collisions.[11,12] There is a basic ambiguity in whether the Si and Si_2 species should be treated as condensed phase particles or as

gas molecules. Schematically, the reaction can be written as either:

$$nSiH_4 \rightarrow nSi(g) \rightarrow \ldots \rightarrow mSi(n/m)$$

or

$$nSiH_4 \rightarrow \frac{n}{2} Si_2(g) \rightarrow \ldots \rightarrow mSi(n/m) \quad .$$

Sawano[11] applied Smoluchowski's[13] average particle size solution of the coagulation equations to the laser process, and found that the agreement was reasonable. Recently Lee has used the concept of self-similarity in the evolving particle size distribution to develop a closed solution that predicts not only the average particle size of an aerosol, but its distribution as well.[14,15] For a case where relaxation to spherical shapes is fast, Lee's principle results are that the average particle volume increases as the 6/5 power of time, and that the particle size distribution rapidly converges to a log-normal distribution with a width parameter of about 1.3.

b. Final Average Particle Size

In the coalescence model, particle growth occurs by two particles colliding and coalescing. Usually, coalescence only goes to completion in the short time scale of these reactions if the particles are liquids. Lee's solution is for a collection of liquid particles. In the laser process, coalescence will proceed from the time the particles melt until they have cooled and solidified or carburized. Large, cold solid particles will not form strong interparticle bonds. The final average particle size is therefore determined in part by the length of time the unreacted Si particles are hotter than the melting point of silicon.

Experimentally this time interval is related to the peak reaction temperature, since increasing maximum temperatures give longer times above

the melting point. The time interval is also related to the velocity of the reactants through the cell since the faster the reactants move through the laser beam, the shorter is the time they spend at high temperature.

The final particle size also depends on the cell pressure which determines the mass density of silicon in the reaction zone. Since the number density decreases at a rate that is not strongly dependent on the mass density, but rather depends mostly on the number density itself, a higher initial mass density will result in larger particles being present at any given time. Higher cell pressures also usually produce higher peak reaction zone temperatures, which result in larger average particle sizes, as described above.

c. Particle Size Distribution

Lee's solution predicts the ultimate emergence of a log-normal size distribution with a width parameter approximately equal to 1.3. The laser process would produce such a narrow distribution only if all of the flow streams remained above 1410°C for the same length of time and they had the same composition. Unfortunately, at the present time the outer edge of the reaction zone is colder than the center and is diluted by the annular stream. Therefore larger particles form in the center of the reaction zone, and smaller ones at the edges. These effects and a non uniform velocity result in a broader distribution; typical width parameters are around 1.7.

2. Formation of SiC Powders by Carburization of Si Particles

We have developed increasing clear evidence that SiC particles form in gaseous mixture of silane and a hydrocarbon through a two-step reaction;

silicon particles form from silane pyrolysis products, and then carburize to produce the silicon carbide particles. This section describes the carburization mechanism of silicon particles. Conversion rates of silicon particles to SiC calculated assuming two postulated rate-limiting mechanisms are compared with experimental results.

a. Background

There are several potential rate controlling steps for the carburization of silicon particles. The most likely were considered to be hydrocarbon pyrolysis or diffusion of Si or C through the SiC product layer. Methane and ethylene were used for SiC synthesis with silane. Pyrolysis kinetics of both gases are reviewed.

Despite the complexity of pyrolysis kinetics, methane's overall reaction rate is believed to be represented by the first-order initiation step:

$$CH_4 \rightarrow CH_3 + H.$$

The rate of pyrolysis is conveniently illustrated using a half life (Table 1) for the reaction.

Ethylene pyrolysis proceeds through parallel channels to form C_2H_2 and C_2H_3. As these reactions are second-order, the rate depends on the initial concentration. For comparison, an equivalent half life of ethylene at the conditions used in our experiments is listed in Table 1 along with the half lives of methane and silane. Ethylene exhibits an intermediate pyrolysis rate between methane and silane.

Table 1. Decomposition half-lives of ethylene, methane and silane (sec).

Temp(K)	C_2H_4 Skinner[16]	CH_4 Chen[17]	SiH_4 Coltrin[18]
1000	125	1.82×10^{7}	0.01
1300	6.2×10^{-2}	190	4.2×10^{-5}
1600	2.1×10^{-3}	0.146	9.6×10^{-7}
1900	2.09×10^{-4}	1.08×10^{-3}	9×10^{-8}

Except grain boundary diffusion of Si, diffusion coefficients of Si and C through different paths have been reported. Carbon grain boundary diffusion is much faster than either of the lattice diffusion paths. Although Si grain boundary diffusion coefficients are not known, the relative values can be deduced. Carburization of silicon substrates by flowing hydrocarbons reveals that material transport through the product layer occurs by silicon grain boundary diffusion. Thus, silicon grain boundary diffusion is faster than that of carbon.

b. Experimental Results

Experiments were performed using the reaction cell shown in Figure 2 and 180 W focused CO_2 laser beam. Both silane and hydrocarbon flow rates were controlled by mass-flow controllers. The ranges of investigated process conditions are summarized in Table 2.

Table 2. Range of process conditions investigated for SiC powder synthesis studies.

Cell Pressure (atm)	0.2 - 0.95
Laser Power Intensity (W/cm^2)	2,500 - 24,000
Silane Flow Rate (cc/min)	10 - 50
Gas Mixture Stoichiometry (C/Si)	0.86 - 2.2
Reaction Temperature (K)	1330 - 2210

1) Methane: Silane System

At 0.95 atm pressure and 6000 W/cm^2 laser intensity, the reaction temperature increased abruptly with decreasing reactant gas flow rates. This phenomenon is referred to as "ignition" (Figure 4). Ignited reaction zones contain two regions. The lower edge of the reaction zone had a crescent shaped region having an orange color, which is called a cusp. The cusp is located below the CO_2 laser beam. The second, upper region of the reaction zone becomes highly luminous at the position of the CO_2 laser beam. This point corresponds to the maximum temperature. Other than temperature, the upper region appeared smooth and continuous throughout the remainder of the reaction zone. Unignited reaction zones do not exhibit a cusp.

The transmittance of a He-Ne laser beam throughout the unignited reaction zone decreased smoothly and monotonically with the distance above the reactant nozzle. In contrast, the transmittance of the ignited plume showed a minimum at the position of the cusp (Figure 5).

The effect of the gas-mixture stoichiometry was examined only for ignited reactions. Excess-methane mixtures were used to obtain stoichiometric SiC powder. The reaction temperature exhibited a maximum at C/Si ratio of 1.27. This maximum is believed due to the competing effects of an endothermic methane pyrolysis reaction and an exothermic reaction to form SiC. The amount of SiC in the powders increased with increasing C/Si ratio of gas mixture; it neared 100% with gas C/Si ratio of 1.67 (Figure 6).

X-ray diffraction analysis revealed that powders produced from unignited reactions consisted primarily of silicon and a small amount of SiC (20%). Ignited reactions produced powders containing a much higher proportion of SiC (70%).

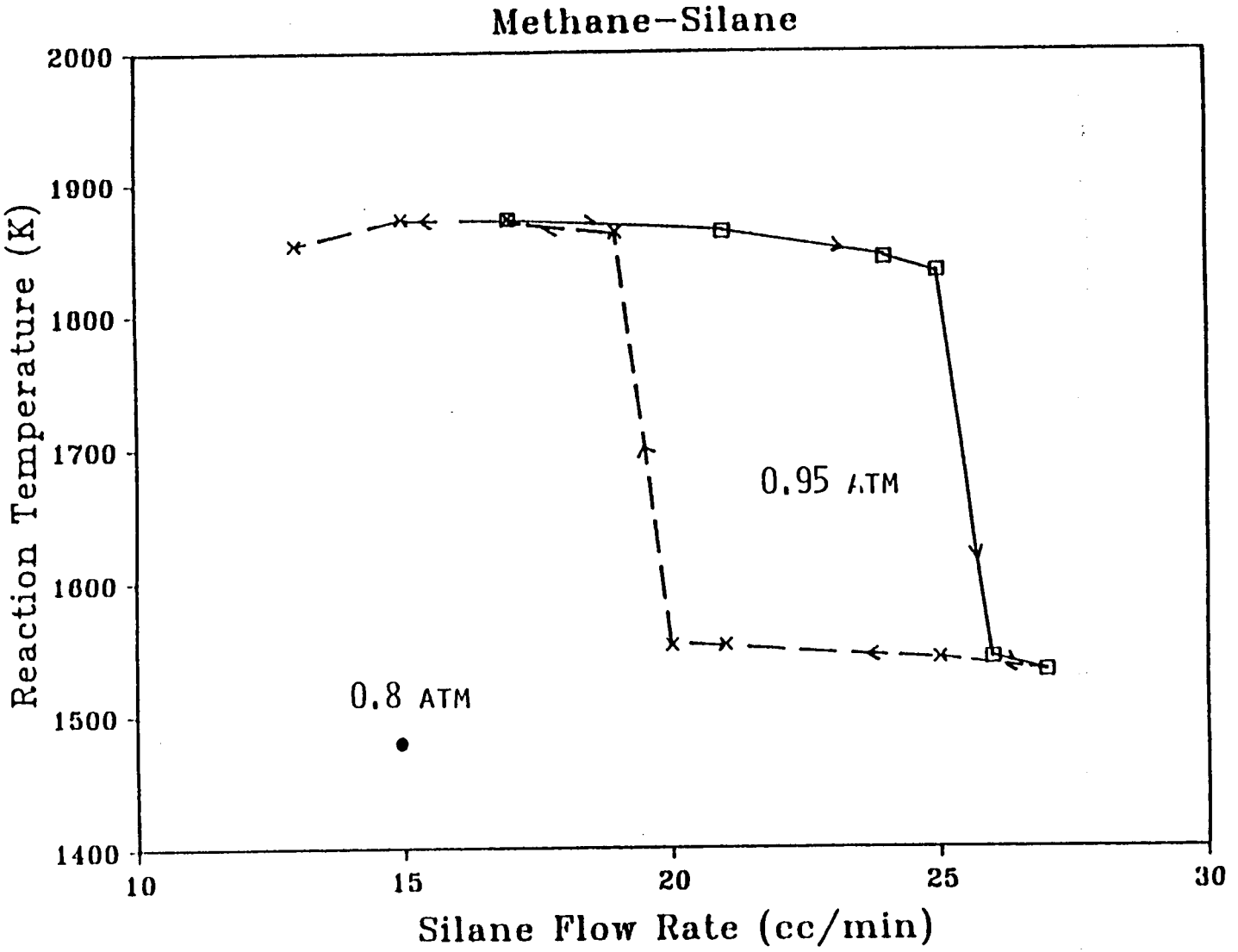

Figure 4. Reaction temperature change versus flow rate at 0.95 atm and 0.8 atm for the CH_4-SiH_4 system. Arrows indicate the direction flow rate change.

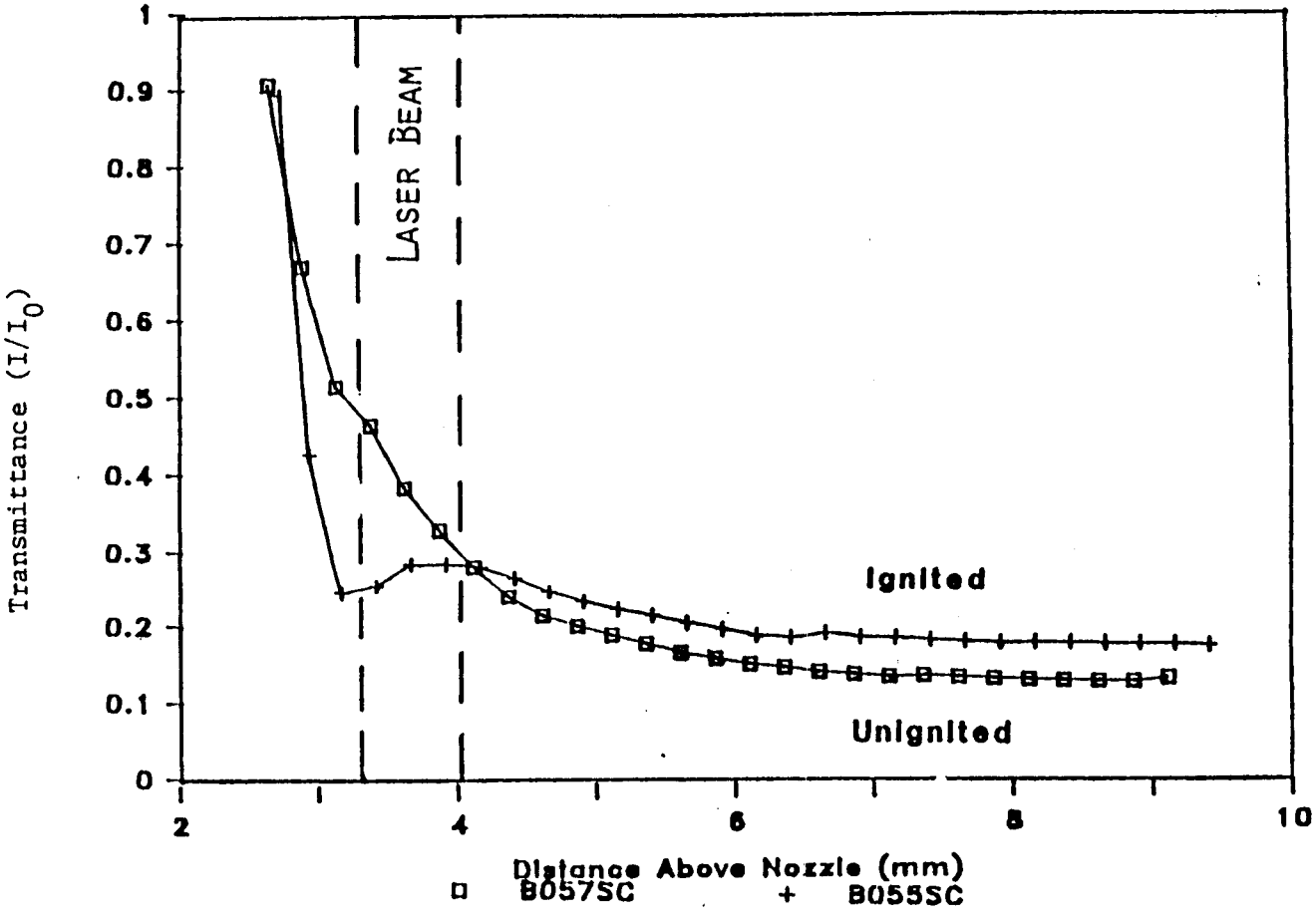

Figure 5. Transmittance profiles of He-Ne laser light through the reaction zone for ignited and unignited plumes.

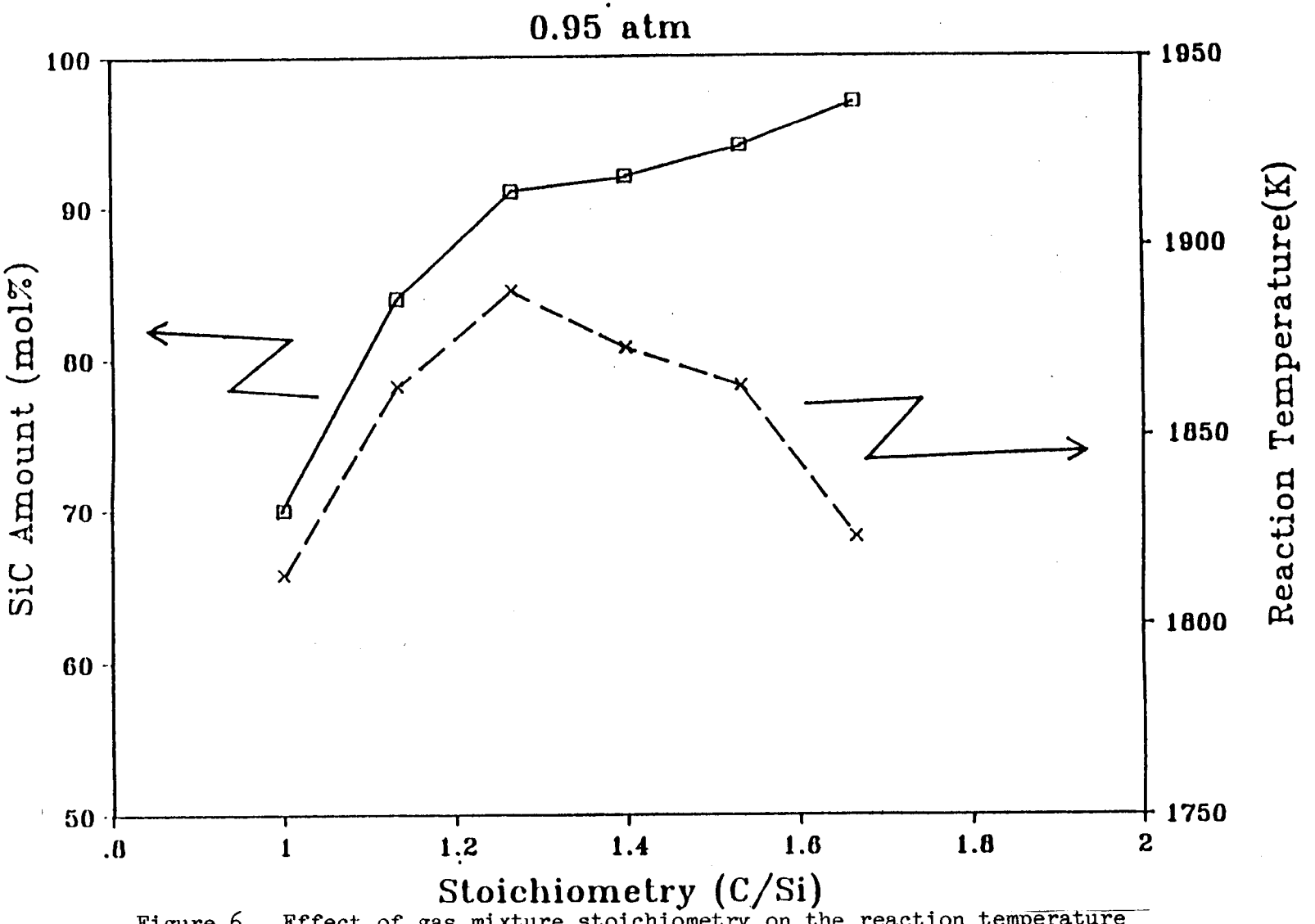

Figure 6. Effect of gas mixture stoichiometry on the reaction temperature and the yield of SiC in powders synthesized from SiH_4-CH_4 gas mixtures. SiH_4 flow rate was fixed at 15 cc/min.

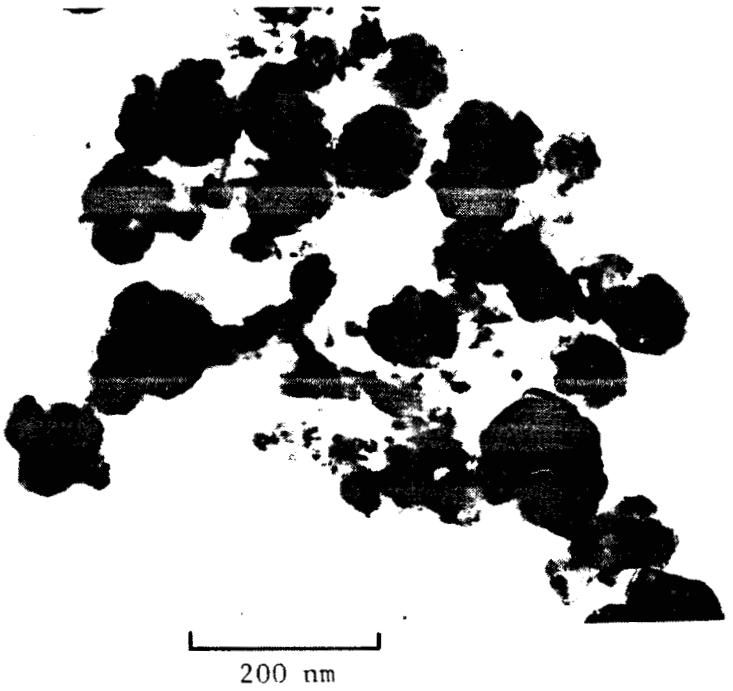

Figure 7. TEM photomicrograph of an ignited-reaction SiH_4-CH_4 powder synthesized at 0.95 atm and 1870K. Particles larger than 1000 Å are observed and are not strongly agglomerated.

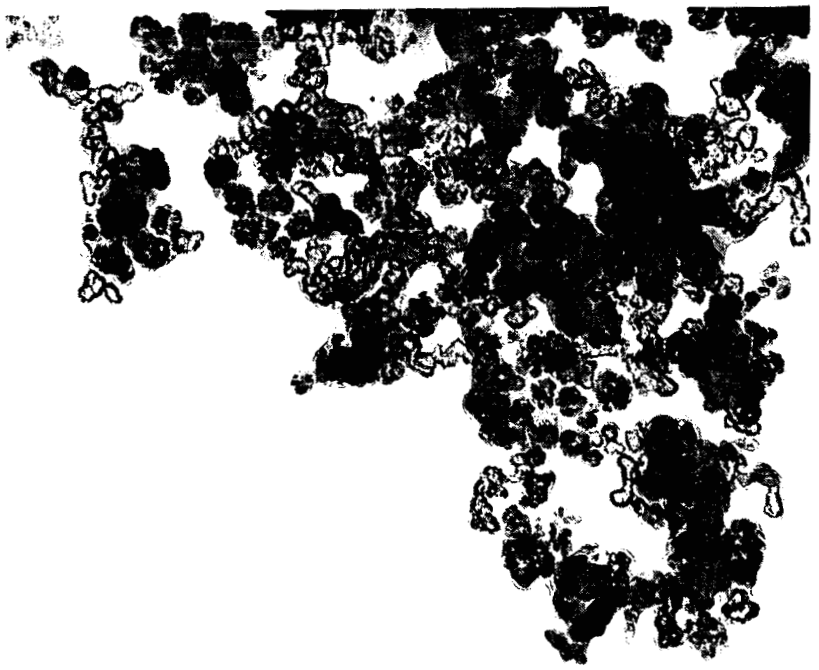

Figure 8. TEM photomicrograph of powder containing hollow particles synthesized at 0.95 atm and 1820K with SiH_4 15 cc/min and CH_4 25 cc/min.

The unignited reaction powders were mostly comprised of agglomerated, medium sized (about 500 Å) particles which were silicon. The ignited reaction powders contained considerable numbers of large particles (>1000 Å) similar in size to large silicon particles which were observed in the high-temperature silicon synthesis runs ($T_{max} \approx 1300°C$). These large particles are polycrystalline and are not agglomerated (Figure 7).

Particle size was measured by TEM and BET. Particle size decreased with increasing C/Si ratio despite the increase of reaction temperature. A remarkable feature was the emergence of hollow particles with increasing C/Si ratios. The interiors of these particles were more transparent to the TEM beam than their outer boundaries. Hollow particles existed only in the medium size range (about 500 Å). No hollow particles larger than 1000 Å in diameter were observed (Figure 8).

2) Ethylene: Silane System

SiC powders were also synthesized using ethylene as a carbon source. As described in the background section, ethylene decomposes faster than methane but slower than silane. The half life of ethylene at temperatures of interest is approximately one hundredth that of methane.

An ignition phenomenon was also observed with the ethylene-silane system; however, the ignition conditions differed from the methane-silane system. Ignition starts with conditions as low as 0.5 atm, 20 cc/min of silane and 6000 W/cm^2 of laser intensity. Unlike the methane-silane system, there was no hysteresis in the process conditions that produce ignition. The fully ignited and unignited reaction zones were indistinguishable from the corresponding methane-silane reaction zones. A cusp was observed in the fully-ignited reaction zones.

characteristic size of remaining flaws should be approximately that of the particles since individual particle vacancies are the largest probable defect.

Our research has demonstrated that the powders must have the following ideal characteristics: (1) the powder must have a small particle size, typically less than 0.5 μm; (2) the powder must be free of agglomerates; (3) the particle diameters must have a narrow range of sizes; (4) the morphology of the particles must be equiaxed, tending toward spherical shapes; (5) the powders must have highly controlled purity with respect to contaminants and to multiple polymorphic phases. Either with the ordered structures shown in Figure 1 or random close packed structures, a powder exhibiting these ideal characteristics should be sinterable to theoretical density without resorting to pressure or additives and should permit the final grain structure to be highly controllable.

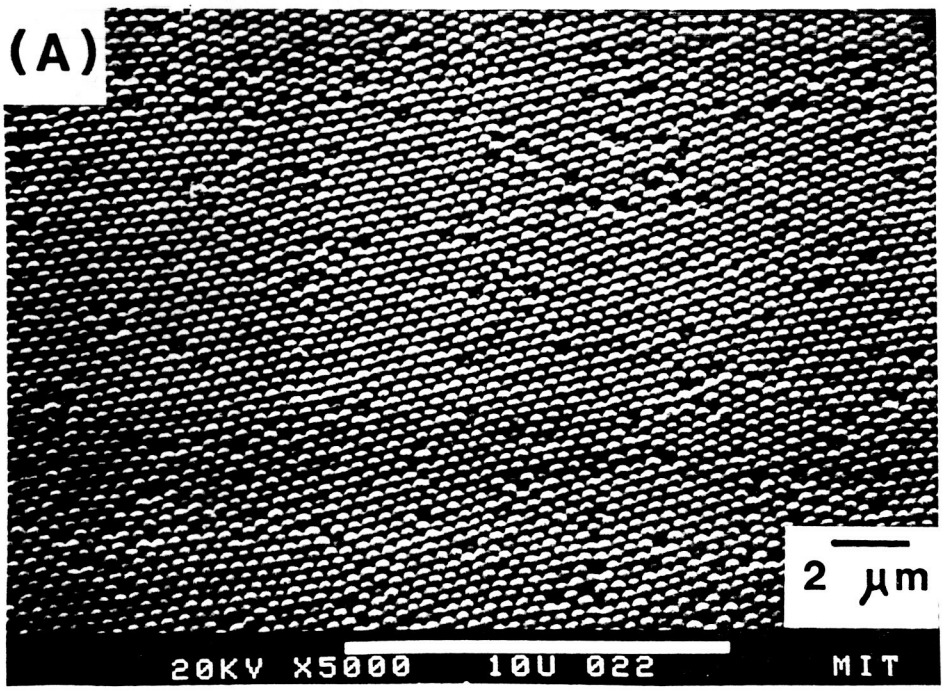

Figure 1. Ordered packing of monodispersed 0.2 μm diameter TiO_2 spheres. (Barringer Ref. 24)

TEM observations showed differences between the microstructures of ethylene and methane derived powders. The most remarkable difference was an absence of the large particles (>1000 Å); thus the average particle size was smaller than that of corresponding methane derived powder. Particles in the ethylene derived powder (Figure 9) appeared to be more agglomerated than those of the methane derived powder.

c. Discussion

As described in the background section, the silicon particle carburization rate is believed to be controlled either by the hydrocarbon pyrolysis rate or by the rate Si diffuses through the SiC product layer. Observed rates were compared with calculated values to identify the operative rate controlling mechanism.[11]

1) Solid State Diffusion

The time for converting a silicon sphere with radius R to SiC with thickness of $(R - r_c)$ is:

$$t = \frac{\rho_B R^2}{6D\Delta C}\left[1-3\left(\frac{r_c}{R}\right)^2 + 2\left(\frac{r_c}{R}\right)^3\right]$$

where r_c is the remaining silicon core radius, ρ_B is the density of silicon, D is the diffusion coefficient of the fast species, and ΔC is the concentration gradient between particle surface and Si-SiC interface. For the ignited reaction, the calculation result using carbon grain boundary diffusion coefficient is higher than the experimental result (Figure 10). Considering that silicon grain boundary diffusion is faster than that of carbon, the difference between the calculated value and the experimental

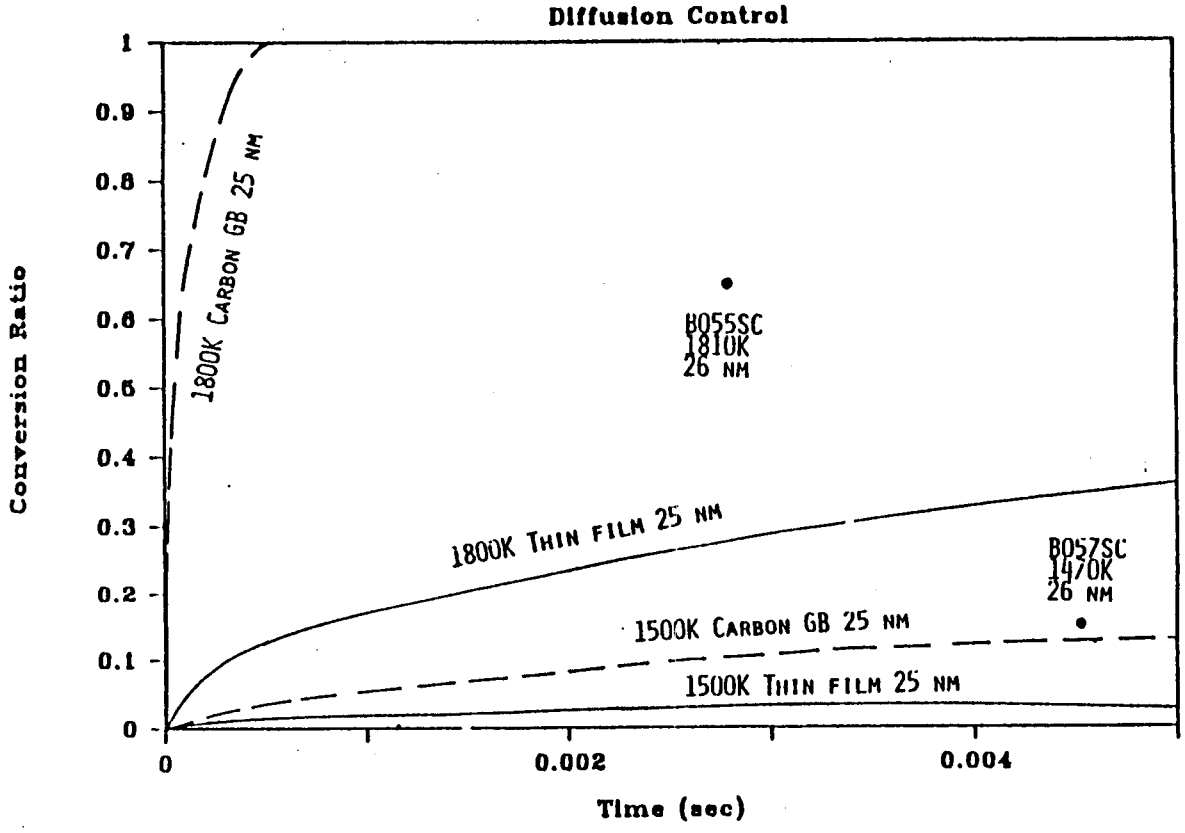

Figure 10. Conversion ratio of a silicon particle to SiC calculated by a diffusion-control model. Carbon GB and thin film designate the grain boundary diffusion coefficient of carbon and the diffusion coefficint obtained from SiC thin film formulation experiments respectively. The numbers are initial radii of particles. For powder synthesis experimental results, reaction temperatures and particle radii are shown with run numbers.

result will differ more. Therefore, the rate-limiting step is not solid-state diffusion for stoichiometric ignited reactions.

2) Methane Pyrolysis

The second calculation assumes that methane pyrolysis is rate controlling. Assuming that decomposed methane immediately reacts with silicon, the conversion ratio to SiC, x, is described by:

$$x = m(1-\exp(-kt))$$

where m is the ratio of methane to silane and k is the rate constant for methane pyrolysis. Figure 11 shows that the calculations agree with the experimental results. Consequently, for a stoichiometric gas mixture, the overall rate-limiting step is most likely to be the methane pyrolysis rate.

3) Hollow Particles

With increasing C/Si ratio in the gas mixture, the overall rate controlling step probably changes to diffusion control as hollow particles appear. The existance of hollow particles indicates that the rate-limiting step is outward diffusion of silicon through the SiC product layer. Also, the use of a rapidly decomposing hydrocarbon such as ethylene should tend to form hollow particle as is the case with excess methane.

Rapid hydrocarbon pyrolysis and carburization at low temperatures is expected to prevent silicon particles from growing by coalesence. Thus, adding excess methane or replacing it with ethylene should produce smaller, agglomerated SiC particles. This was observed in the experiments.

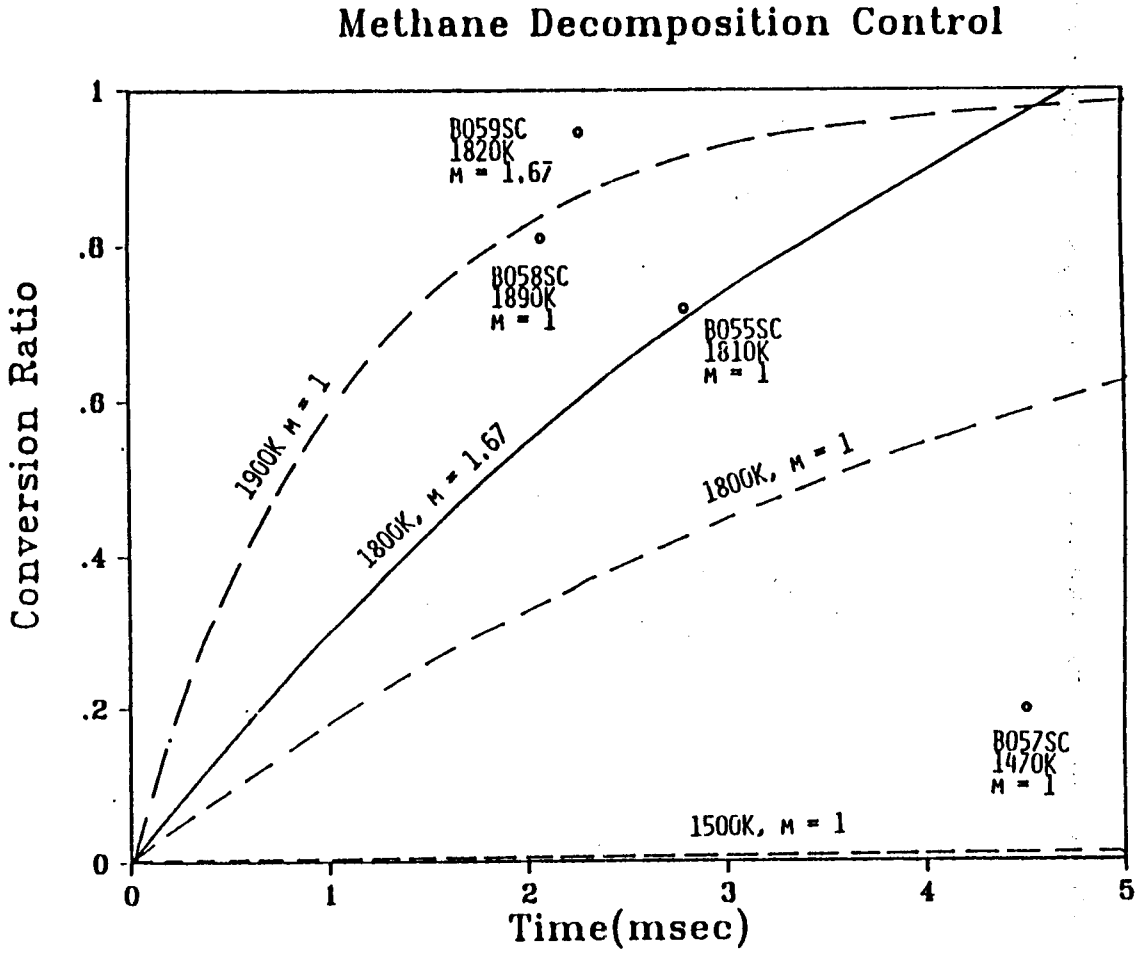

Figure 11. Conversion ratio of silicon particles to SiC calculated by the methane pyrolysis control model where m designates C/Si molar ratio. Powder synthesis experimental results are plotted with run numbers, temperatures, and C/Si molar ratios in the gas mixtures.

d. Approach for Producing an Ideal Powder

The understanding of the formation mechanism provided a rational basis for producing an ideal SiC powder by this process. Silicon particles must grow to final dimensions before carburization begins, since SiC particles cannot coalesce. The silicon particles must therefore grow before the pyrolysis of the hydrocarbon becomes rapid, so a slowly decomposing hydrocarbon is desirable, that is, methane. An "ignited" reaction condition must be achieved with the smallest amount of methane that will yield stoichiometric powder. If possible, it would be best to add the hydrocarbon into the stream after appropriate growth of the silicon particles.

C. Silicon Carbide Powders: Current Status

We are now routinely producing significantly improved silicon carbide powders using the approach described above. The new powders are larger (average particle diameter of ~900Å) and have fairly narrow particle size distributions (log-normal width parameter of around 1.6). The particles are spherical, non agglomerated, and can be made stoichiometric, or if desired, 1-2% carbon rich. This powder disperses well, and can be packed to green densities of 60% or more. This new powder contrasts strongly with initial SiC powders[8], which were characterized by smaller sizes, hard agglomerates, and imprecisely controlled stoichiometry.

We can explain the improvement in powder properties using the collision/coalescence model and the two-step model. The new powders are larger because they are produced at higher pressures, with correspondingly higher initial silicon density. At these higher pressures, larger silicon

particles grow before carburization begins, so the final SiC particles are larger. This is only possible if methane is used for the carbon source, as explained above.

The particle size distribution is more narrow because all of the flow streams pass through an intense portion of the laser beam. Previously, only 180 watts of laser power was available. To achieve ignition, the laser was focussed to a 2 mm diameter spot. Some of the reactant gas therefore flowed around the beam. These flow streams produced very different powder from the flow streams that experienced the high intensity of the focussed laser beam. With the present apparatus, we have up to 400 watts available. The beam is focussed to a 2 mm high by 5 mm wide elipse, which is wide enough that all of the flow streams pass through intense laser irradiation. The particle size distribution would be even more narrow if the laser intensity could be made more uniform across its 5 mm width.

We are now making stoichiometric (or on demand carbon rich) SiC because all of the flow streams are being ignited. The particles are not agglomerated because the silicon growth zone is distinct from the carburization zone. Once carburization begins, the particles get coated with a layer of SiC that prevents colliding particles from sticking since even at 1800°C the SiC is solid. In this way, the collision/coalescence model remains consistent with a 1000Å average particle size. Pure silane reactions at similar flow rates and pressures produce 3000Å powders. This is because particle growth continues until the particles flow out of the laser beam and cool below 1410°C, the silicon melting point.

Finally, the improved dispersion and packing behavior of the new powder is a consequence of the above listed properties. The particles are large

enough that interparticle forces can be overcome using the proper dispersants. Since there are no hard agglomerates, the powders can be pressed to high green densities. The excess carbon content can be controlled for sintering studies. We have succeeded in developing the silicon carbide laser synthesis process into a source of unique, high quality silicon carbide powder.

IV. DISPERSION OF SiC POWDER

A. Introduction

To produce flaw-free, high quality ceramics control of all processing steps including powder preparation, fabrication, sintering and finishing is required. Powder preparation techniques normally include grinding and purification of Acheson SiC. Much work has been done[19,20,21] characterizing the flaws associated with ceramic parts manufactured from comminuted silicon carbide powders with broad particle size distributions. It appears that this approach falls short of the goal of high quality parts. Hermansson[22] has demonstrated that high green densities, reduced sintering cycles and improved microstructures are possible by utilizing submicron SiC particles with a narrow size distribution. His failure to deomonstrate improved properties may have been due to departures from ideality[23] because these powders were non-spherical and impure. The laser synthesis process[6] is capable of producing SiC powders that adhere more closely to the concept of ideality.

Highly perfect green compacts have been formed from "ideal" oxide powders dispersed in a liquid medium[24]. It appears possible that this approach may be exploited by applying the commercially popular techniques of

slip casting and injection molding to dispersions of ideal SiC powders. The advantages of these techniques include formation of complex shapes and high density green compacts. Whether these fabrication techniques can be used to process laser synthesized SiC powder depends first on developing dispersing systems.

Dispersing systems must preserve purity and must facilitate processing at all stages. The formation of an oxide layer on SiC powder has been observed[25] for aqueous powder dispersions. It has been shown[26] that oxygen levels >0.2 wt.% degrade the high temperature strength of SiC. In addition, the processing of submicron silicon bearing ceramic powders in aqueous media is hampered by the formation of silica slimes which prevent the achievement of high green density compacts.[27] For these reasons SiC is normally dispersed in non-aqueous mediums. Of these, the obvious contaminant bearing systems were not considered (e.g., alkali, sulfur and phosphorus containing compounds). The remaining systems were evaluated for their powder dispersing capabilitites.

For nearly perfect microstructures to be formed from a dispersion of ceramic particles, the particles must remain isolated in the medium until added singlely to the forming compact. The first criterion to be met is that the medium wet the powders[28,29]. Secondly, normal mechanical aggitation is sufficient to break up flocs formed in the dry powder. Ultrasonication is an excellent way of doing this[30,31]. Finally the particle must be kept isolated in the liquid medium by interparticle repulsion. Such a dispersion is said to be stable and may be achieved by either of two approaches, coulombic stabilization or steric stabilization. Coulombic stabilization is effected by the repulsion between particles

resulting from the interaction of overlapping ionic charge clouds (double layers) during particle-particle approach[32]. Steric stabilization is due to the increase in free energy associated with the interpenetration of marginally soluble macromolecules adsorbed on the particle surface[33].

This chapter deals with these dispersion issues.

B. Dispersion in Non-Aqueous, Pure Solvents

Silicon carbide powders synthesized from laser driven reactions have extremely pure surfaces because of the synthesis process and handling procedures. Consequently, the surfaces of laser silicon carbide powders differ from those of commercial silicon carbide powders, which are generally known to have slightly oxidized layers on their surfaces. Because the dispersion characteristics of powders are strongly dependent on their surface characteristics, the laser silicon carbide powders are expected to behave differently from commercial silicon carbide powders. Understanding dispersion characteristics in pure solvents is needed not only for choosing an effective pure solvent, but also for identifying a good dispersant.

The dispersion characteristics of pure silicon powders made from laser heated SiH_4 were previously studied[9] and ascertained to depend on the dielectric constant of solvents. This research concentrated on pure solvent systems in the absence of dispersants[34] to confirm their applicability to fine, pure silicon carbide powders made by the laser synthesis process and to understand the powders' dispersion characteristics.

1. Experiments

a. Materials

Three types of pure laser synthesized SiC powder made under different conditions, one commercial SiC powder (IBIDEN BETARANDOM ULTRAFINE), and an oxidized laser powder were used in this study. Their synthesis conditions are given in Table 3 and characteristics are summarized in Table 4.

Oxidized laser SiC powder was prepared by heating laser SiC powder L014 in air at 600°C for 5 hours after breaking the soft agglomerates with a 30 minute exposure to a 40 watt ultrasonic probe with the powders dispersed in isopropyl alcohol. The oxidized laser SiC powder was characterized with single point BET, TEM, XRD and FTIR. The oxidized powder had approximately the same surface area, morphology and crystal phase as the pure laser powder L014. The only difference was the presence of an oxidized layer on the particle surfaces.

Commercially available grades of organic solvent were used in this study (Table 5). These solvents represent commonly available organic families, including aliphatic and aromatic hydrocarbons, chlorides, ethers, ketones, esters, alcohols, aldehydes, carboxylic acids, amines and water. The solvents were dried with a 3Å molecular sieve.

b. Dispersion Test

Simple screening tests and centrifugal castings were used to determine the stability of the SiC powders dispersed in the investigated solvents.[34]

Preparation of suspensions for screening tests was conducted under a nitrogen atmosphere using a glove box. After a small amount of powder (10mg)

Table 3. Synthesis conditions for powders used in pure solvent dispersion studies.

Run Number	Reactant (Carbon)	Laser Power (W)	Reaction Temp (°C)
B038	Ethylene	150	1650
B060	Methane	150	1680
L014	Methane	500	1830

Table 4. Characteristics of powders used in pure solvent dispersion studies.

CHARACTERISTIC	LASER-POWDERS			COMMERCIAL	OXIDIZED L014
	B038	B060	L014		
SPECIFIC SURFACE AREA (m^2/g)	44.9	44.3	22.4	19.4	23.3
BET PARTICLE SIZE (nm)	41.5	42.1	83.1	98.0	80.0
SIZE DISTRIBUTION	narrow			wide	narrow
MORPHOLOGY	spherical			irregular	spherical
SURFACE	pure			slightly oxidized	slightly oxidized
PHASE	β	β	β	β	β

Table 5. Results of screening tests and centrifugal casting tests for pure solvent dispersion studies.

SOLVENT	DISPERSIBILITY		PACKING DENSITY %				H.B.
	PURE	OXIDIZED	B038	B060	L014	COMMERICAL	INDEX
HYDROCARBONS							
1 hexane	P	P	11.9	16.4	20.5	28.4	2.2
2 toluene	P	P	12.8	19.5	23.6	31.0	3.0
CHLORIDES							
3 methylene chloride	G	G	11.8	17.2	23.9	26.8	2.7
4 chloroform	G	G	14.0	17.0	26.8	29.0	2.2
5 carbon tetrachloride	P	P	11.3	16.7	25.9	26.9	2.2
6 1,2-dichloroethane	G	G	14.0	19.8	25.6	29.4	2.7
7 trichloroethylene	P	P	12.8	17.7	25.9	27.7	2.5
8 chlorobenzene	P	P	13.9	18.7	26.2	30.9	2.7
CYANIDE							
9 acetonitrile	G	G	11.1	15.8	25.1	34.8	4.5
ETHERS							
10 isopenthyl ether	G	P	-	25.5	29.0	34.4	(6.0)
11 tetrahydrofuran	G	G	13.6	21.8		34.1	5.3
12 dioxane	P	P	16.1	25.8	28.7	36.7	5.7
KETONES							
13 acetone	G	G	14.7	18.3	26.8	38.0	5.7
14 2-butanone	G	G	15.5	20.7	26.2	34.9	5.0
15 2-heptanone	P	G	-	22.2	27.5	36.9	(5.5)
ESTERS							
16 ethyl formate	P	VG	12.2	22.3	-	33.0	5.5
17 ethyl acetate	G	G	15.0	22.3	26.4	34.6	5.2
ALDEHYDE							
18 benzaldehyde	P	VG	-	26.5	29.5	39.1	5.2
ALCOHOLS							
19 methyl alcohol	P	VG	16.2	24.3	25.0	37.6	8.9
20 ethyl alcohol	P	VG	16.1	25.2	27.7	37.8	8.9
21 n-propyl alcohol	P	VG	16.2	25.1	27.0	37.4	8.9
22 2-propyl alcohol	P	VG	16.3	25.6	30.2	38.6	8.9
23 2-furfuryl alcohol	P	VG	-	-	28.9	38.8	(8.9)
24 benzyl alcohol	P	VG	-	25.1	31.2	41.5	8.9
25 n-octyl alcohol	G	VG	-	26.4	32.4	38.4	8.9
26 ethylene glycol	G	VG	-	15.4	22.8	39.0	9.6
AMINE							
27 propylamine	P	VG	12.7	21.8	28.3	40.2	9.0
CARBOXYLIC ACID							
28 propionic acid	G	P	-	21.0	27.4	35.9	9.5
29 n-octanoic acid	G	VG	-	22.7	29.7	39.9	9.5
30 oleic acid	VG	G	-	22.3	25.7	32.4	9.5
INORGANIC							
31 water	F	G	11.0	16.5	20.3	36.8	

P: poor dispersion
G: good dispersion
VG: very good dispersion
F: flotation

was mixed with the selected solvent ($10cm^3$), the powder was dispersed by subjecting the suspension to a 40 watt ultrasonic probe for two minutes. After standing for 5 days, the stabilities of the suspensions were evaluated visually.

Centrifugal casting experiments also provided an expedient means of evaluating the dispersions; e.g., good dispersions yield high packing densities. Suspensions consisting of 290mg of SiC powder and $9cm^3$ of investigated solvents were prepared under a nitrogen atmosphere in a similar manner as above. The suspensions were centrifugally cast at 3000 g's for 2 hours. The sediment volumes were determined by measuring their heights with a scale in the centrifugal tubes; the height-volume relationship had previously been calibrated with a syringe. After drying the sediments in a nitrogen atmosphere, sediment weights were measured to permit calculation of their packing densities. The microstructures of these sediments were observed with a scanning electron microscope.

Colloidal pressing was also used to make green compacts from suspensions using selected solvents. The packing densities of these compacts were measured and the microstructures were obeserved with SEM.

2. Results

a. Screening Test for Dispersibility

The results of suspension screening tests were evaluated and were classified into the following four ranks:

- Very good dispersion (designated VG): most of the particles remained well dispersed after several days.

- Good dispersion (designated G): some particles remained well dispersed, while others (~1/2) settled out of the suspensions after several days.
- Poor dispersion (designated P): most of the particles settled out of the suspensions within one day.
- Particle floatation (designated F): most of the powder floated on the solvent surface. The particles could not be incorporated into the liquid, even after vigorous agitation. This phenomenon was observed only for the combination of water and pure laser powder.

Significant differences in dispersibility were observed between pure laser powder and oxidized laser powder as shown in Table 5 but not between specific pure powder types. In the case of pure laser powders, "very good" dispersion was observed only for oleic acid. "Good" dispersion was observed for the other carboxylic acids (such as propionic acid and n-octanoic acid), high molecular weight alcohols (such as n-octyl alcohol), ethylene glycol etc. On the other hand, oxidized laser powders dispersed very well in many kinds of solvents such as all alcohol groups, propylamine, ethyl formate and octanoic acid.

b. Centrifugal Test

Packing densities of centrifugal sediments are also given in Table 5 for several solvents. Packing densities were directly related to the liquid functional group and the specific powder type.

For pure laser powders, octyl alcohol showed the highest packing densities. However, the packing densities from oleic acid was not very high; it was the best solvent in the screening test. A strong correlation between centrifugal packing densities and screening test results was observed for the commercial powder which had an oxidized layer, while some exceptions were observed for pure laser powders. These exceptions may be attributed to the relatively lower dispersibilities of the pure laser powders. The average packing densities of the laser powders increased in the following order; B038, B060, L014. The commercial powder exihibited a higher average packing density than the laser powders.

c. Dispersibility and Solvent Characteristics

Dispersibility in the examined systems may be attributed to the formation of electrical double layers resulting from surface-liquid interactions. These interactions are defined by the powders' surface characteristics and functional groups of the liquid molecules.

Packing densities of centrifugal sediments as a function of hydrogen bond indexes of the solvents are shown in Figure 12. Hydrogen bond indexes were derived from chemical shifts of spectroscopic data obtained by Gordy's technique. Good correlation was observed between packing densities of all powders and hydrogen bond indexes. High hydrogen bond indexes provided high packing densities. Good correlations between hydrogen bond index and screening test results were also observed for the oxidized powder. However, screening test results for the pure powders and the differences in dispersibilities between pure and oxidized powders could not be interpreted only by hydrogen bond strengths.

Table 6. Comparison between dispersibilities of pure laser powder and oxidized laser powder.

		DISPERSIBILITY FOR OXIDIZED POWDER		
		POOR	GOOD	VERY GOOD
	POOR	HYDRO CARBONS CHLORIDES ETHER	KETONE	AMINE LOW-ALCOHOLS ESTER ALDEHYDE
	GOOD	ETHER CABOXYLIC-ACD	KETONES ESTER ETHER NITRILE CHLORIDES CARBOXYLIC-ACID	HIGH-ALCOHOLS
	VERY GOOD	CARBOXYLIC-ACID		

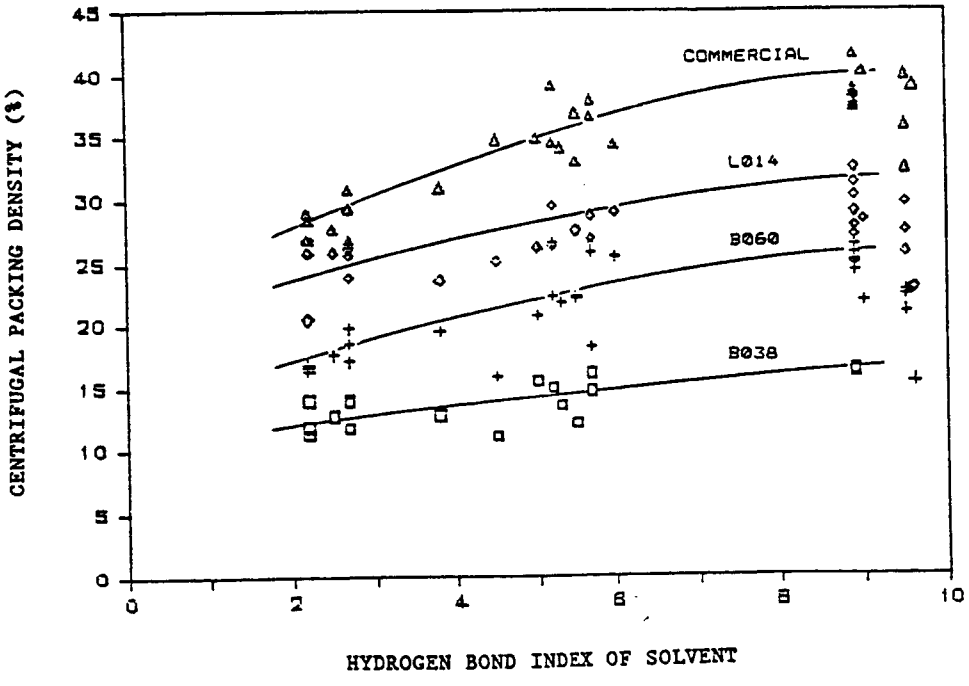

Figure 12. Centrifugal packing densities as a function of hydrogen bond indexes of solvents.

The comparison between dispersibilities of pure laser powders and oxidized laser powders are shown in Table 6 for the families of organic solvents studied. Some solvent families, such as carboxylic acid, amine, etc., showed different dispersibilities depending on the specific powder type and member of the solvent family. These phenomena may be related to the acidity and basicity of the solvents and powder surfaces.

Propylamine and low molecular weight alcohols, which act as Lewis bases, dispersed oxidized laser powder well; however, they did not disperse pure laser powder well in spite of their high hydrogen bond indexes. In contrast, oleic acid and propionic acid, which act as Lewis acids, dispersed pure laser powder well; however, they did not disperse oxidized laser powder very well. This phenomenon may be attributed to the different interactions between powder surfaces and solvents due to their acidity or basicity. The surfaces of pure laser powders are probably Lewis basic and have good interactions with Lewis acid solvents.

The stability of the suspensions were evaluated in terms of the dielectric constants (ε) of the solvents to see whether high ε solvents favored stable suspensions and low ε solvents tended to give rise to flocculation. No strong correlation was found for pure SiC powders; e.g., propionic acid showed good dispersion characteristics in spite of its low ε. The oxidized powder gave results that were similar to those observed with Si; the dispersion stability improved with increasing dielectric constant of the solvent.

d. Packing Density and Powder Characteristics

Significant differences between the centrifugal sediment densities were observed among four kinds of powders: B038, B060, L014 and commercial powder.

These differences should be attributable to powder characteristics such as particle size, particle size distribution, particle morphology, aggregation and dispersibility. Packing density should be independent of particle size, if the particles are large enough to eliminate the influence of electrostatic forces, surface films, boundary effects, etc. Increased width of particle size distribution increases packing density. High aspect ratio particles such as plates, rods, etc., pack to higher densities than spheres as a result of orientation. Spheres can pack most uniformly. Agglomerates and aggregates generally (but not always) have lower packing density than randomly packed individual particles.

The packing densities achieved with the type L014 powder were consistently higher than those achieved with type B038 and B060 powders. Although the type L014 powder was approximately twice as large as the other two, it is unlikely that this difference was responsible for the improved packing density. All three exhibited nominally the same dispersibilities. It is more likely that the B038 and B060 powders consist of aggregated primary particles which can be dispersed but do not pack well. Further research with photon correlation spectrometry should clarify this issue. The high packing densities achieved with the commercial powder may be attributed to wide particle size distribution and morphology.

e. Characterization of the Sediments and Colloidally Pressed Green Bodies

The micrographs of the top surfaces of centrifugal sediments from L014-hexane and L014-octyl alcohol suspensions are shown in Figure 13. These packing densities are 20.5% and 33.2%, respectively. The particles dispersed in octylacohol are packed much better as shown by fewer numbers of large voids and loosely packed agglomerates.

Micrographs of a fracture surface and a side surface of a colloidal pressed pellet using octyl alcohol are shown in Figure 14. No voids larger than the particle size are present and several areas show ideal close packing of spheres. The packing density of this pellet was ~62%.

f. Effect of Carboxylic Acid in Solvents

According to a screening test of dispersibility, carboxylic acids, especially oleic acid, were one of the best dispersants for dispersing pure laser powder. However, oleic acid may not be desirable because of its high viscosity and boiling point. Oleic acid was therefore diluted in the other solvents and the solution was evaluated with a centrifugal test (Figure 15a). Steric acid was also evaluated as an additive to the same solvents. The results are given in Figure 15b. Small amounts of oleic acid and steric acid in hexane and chloroform improved the packing density of the sediments over those of the pure solvents.

3. Conclusions

Laser SiC powder showed different dispersibility tendencies than commercial powder because of its pure surface. The dispersibilities of these powders in non-aqueous solvents were related to the acidity/basicity

(a) LO14/Hexane

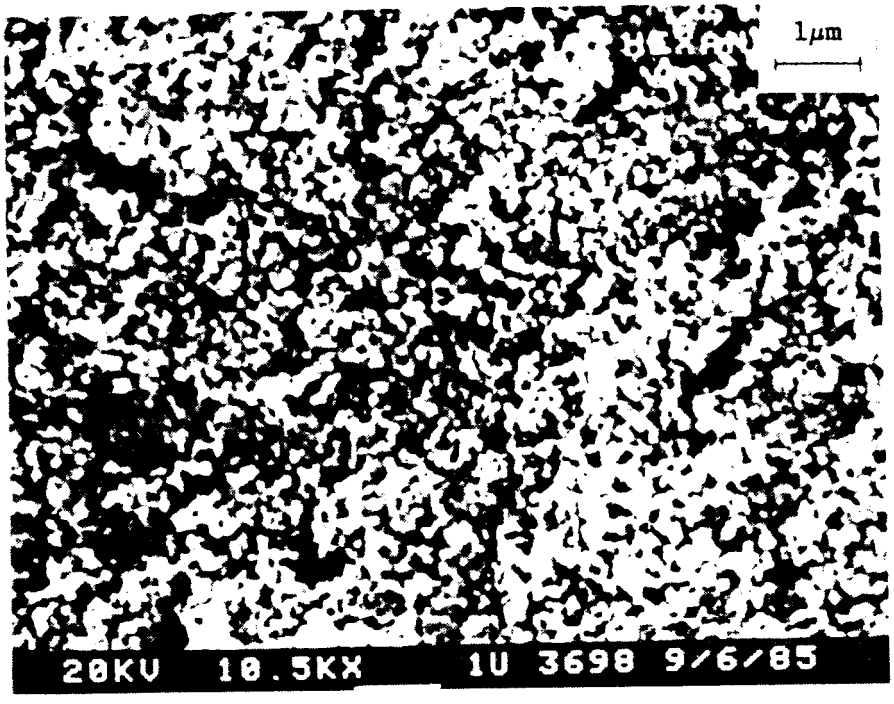

(b) LO14/Octyl Alcohol

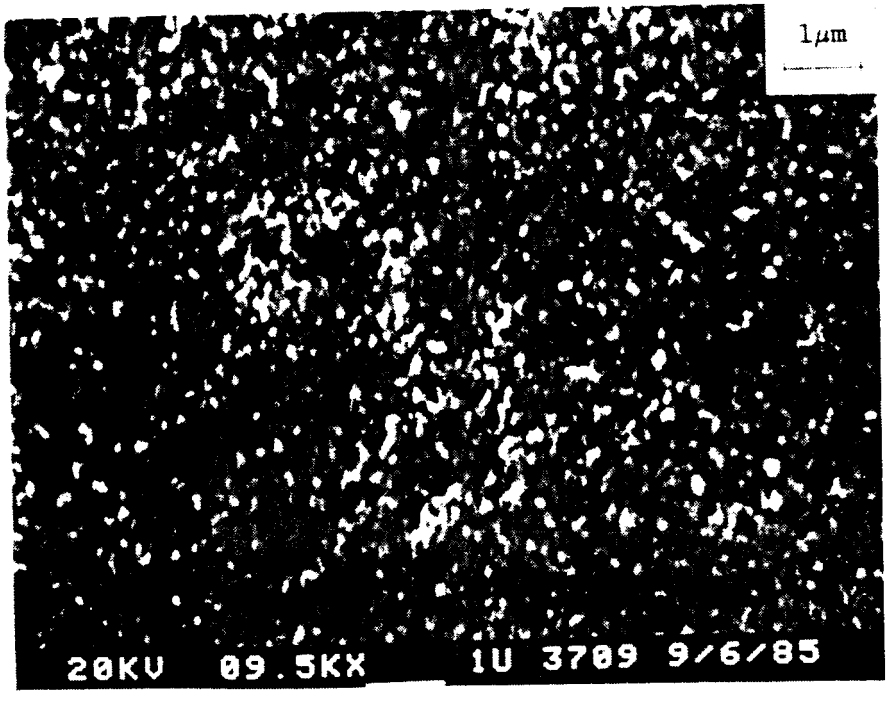

Figure 13. SEM photomicrographs of centrifugally cast SiC sediments from (a) LO14/hexane and (b) LO14/octyl alcohol.

(a) Fractured Surface

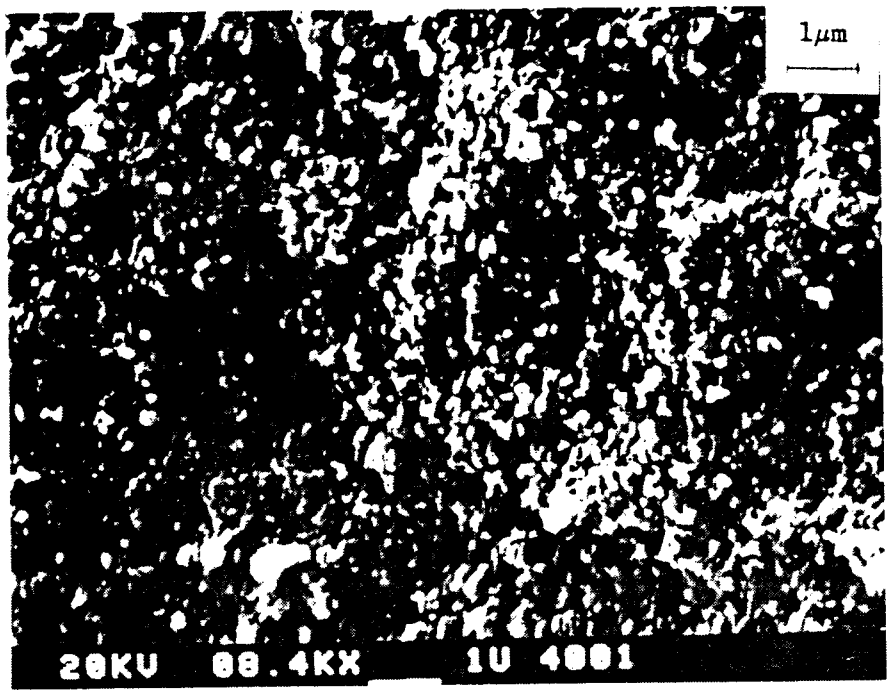

(b) Side Surface

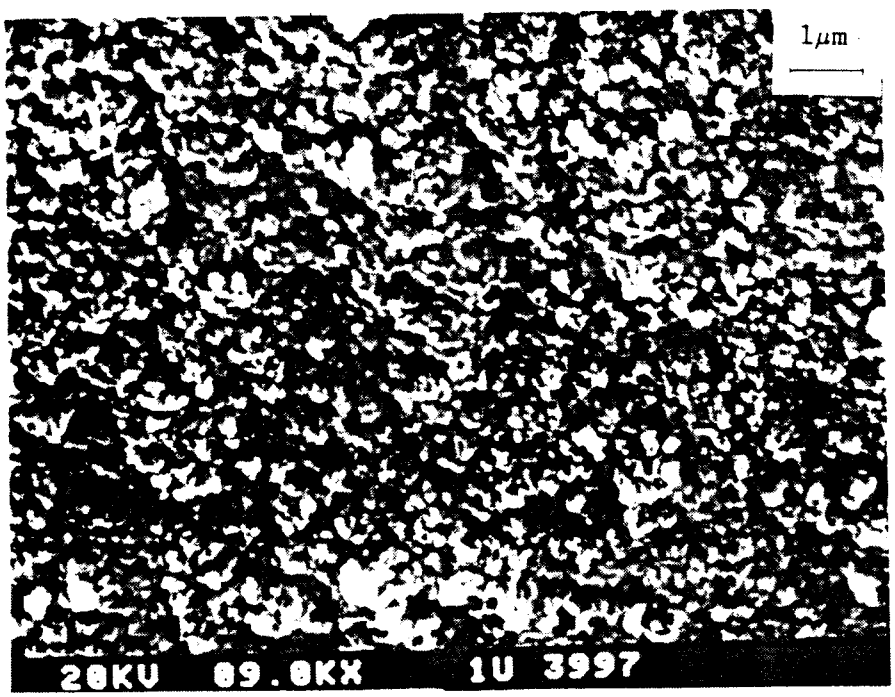

Figure 14. SEM photomicrographs of colloidal pressed SiC compact from L014/octyl alcohol: (a) fractured surface, (b) side surface.

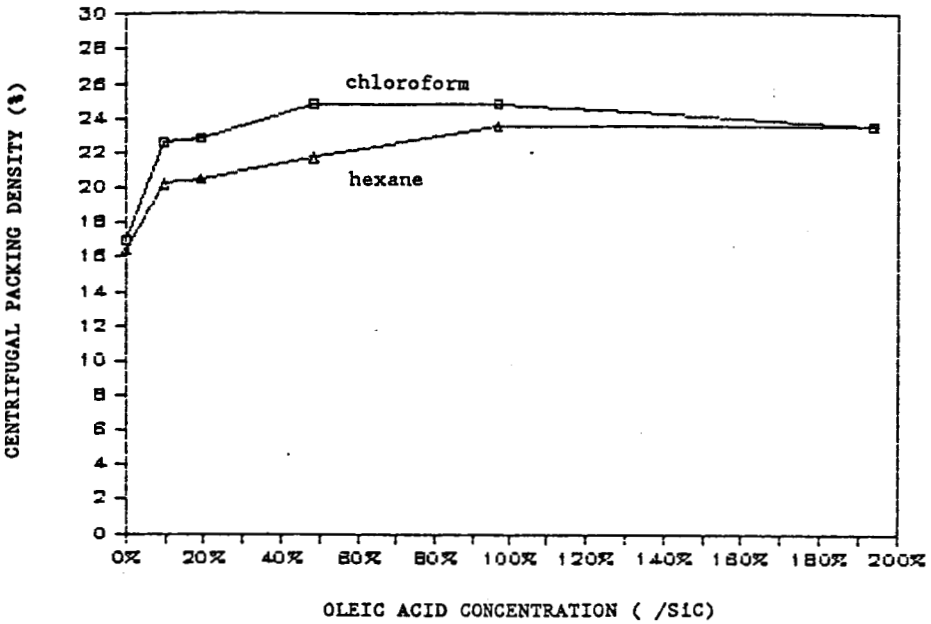

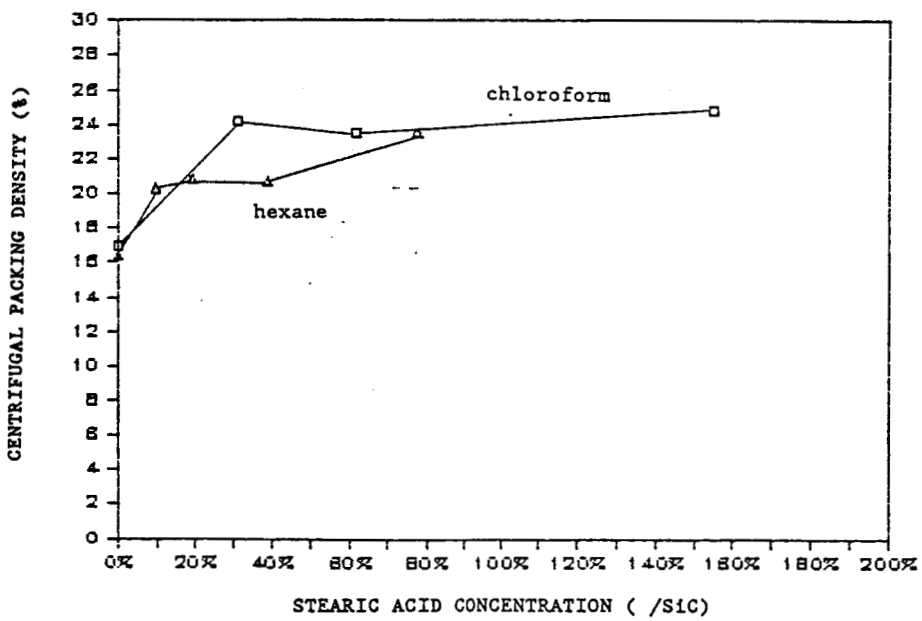

Figure 15. Centrifugal packing densities of powder type B060 as a function of carboxylic acid concentration in: (a) oleic acid, (b) stearic acid.

and the hydrogen bond strength of the solvents. Oleic acid showed the best dispersiblility for laser powder; however it might not be desirable because of its high viscosity and boiling point. Octyl alcohol may be the most suitable pure solvent. Using colloidal pressing with octyl alcohol, uniform and high density (up to 63%) green bodies were obtained.

C. Dispersion of SiC by Steric Stabilization

1. Experiments

a. Systems Studied

Oloa-1200^{TM} was used as a dispersant with hexane. Other dispersants were tested preliminarily by visual inspection; however, none was as effective as Oloa-1200 for laser synthesized SiC.[35]

Nine different laser derived powders were examined in this work. Major differences between powders were attributed to the carbon source and the laser optics; minor differences were attributed to synthesis temperature, gas velocity, etc. Physical properties of the powders which were used in these experiments are summarized in Table 7.

b. Method

Dispersions were prepared under oxygen-free conditions using a glove box. Mixed powders were subjected to a 40 watt, 5 minute ultrasonic treatment to produce a dispersed state.

Table 7. Powder characteristics and synthesis conditions of laser synthesized SiC powders used in steric dispersion studies.

Run Number	Reactant (Carbon)	Laser Power (W)	Reaction Temp (°C)	Surface Area (m^2/g)	BET Equiv. Diameter (nm)
L006	Methane	500	1830	32.1	58.5
G011	Methane	150	1600	53.4	35.1
G010	Methane	150	1615	49.1	38.1
B059	Methane	150	1550	58.2	32.2
B082	Ethylene	150	1310	69.6	26.9
G008	Ethylene	150	1410	67.0	25.9
G009	Ethylene	150	1580	61.9	30.3
B064	Ethylene	150	1940	65.3	22.7
A002	Ethylene	150	N.A	72.4	19.4

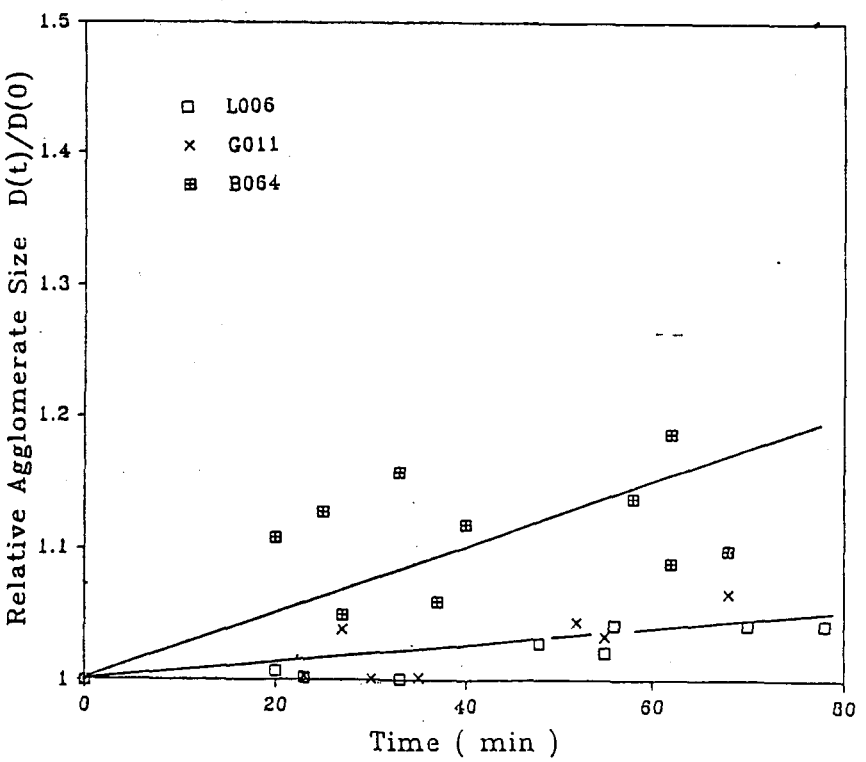

Figure 16. Relative agglomerate size as a function of time after an ultrasonic treatment for three different powders in Oloa/hexane. The initial agglomerate dimension was taken at the end of the fast agglomeration period.

Centrifugal casting was mainly used to evaluate packing ability. Although this technique is good for quick evaluations, it is not effective as a means for making green bodies which are ready to sinter. Therefore colloidal pressing was used for the green body fabrication study.

Agglomerate sizes were determined by photon correlation spectroscopy. Primary particle size and size distribution were measured by BET and TEM. Microstructures of green bodies were examined directly using SEM microscopy.

2. Results and Discussion

a. Agglomerate Size/Time Dependence

Agglomerate size was measured as a function of time after ultrasonic treatment for B064, G011 and L006 powders. Each sample contained $4x10^{-4}$ g/cc to $5x10^{-4}$ g/cc powder and 30 - 40 wt% Oloa-1200 based on powder weight.

Figure 16 shows that the agglomerate sizes increased 5-6% in approximately 1 hr. B064 powder showed a slightly higher coagulation tendency than the other two powders. Comparing these results with similar dispersions in pure hexane (>3000Å 30 sec) shows that Oloa-1200 works as an effective dispersant for the laser synthesized, non-oxidized SiC. However, the results also indicate that the steric barrier formed by Oloa-1200 may not be effective enough to maintain a well dispersed state for a long period.

b. Effect of the Oloa Concentration on Packing Density

It is desirable to minimize the amount of dispersant needed to maintain a dispersed state because the dispersant may remain in the green body after drying and it should be removed completely before firing. The minimum Oloa

requirement was examined by the centrifugal casting method. Samples were centrifugally cast at 3000 g's for 1 hour. The powder concentration in the slips was 1 vol% for each sample.

The results in Figure 17 show that the minimum Oloa requirement is about 20 percent of the powder weight. Assuming 1 Oloa molecule per 100$Å^2$ of particle surface, an absorbed monolayer corresponds to approximately 2% of the particle weight. The excess dispersant probably remains dissolved in the hexane solvent. Preliminary data showed a weak dependence of the critical Oloa concentration on the powder surface area. This is consistent with the weak segregation of Oloa to the particles' surfaces and its high solubility in hexane.

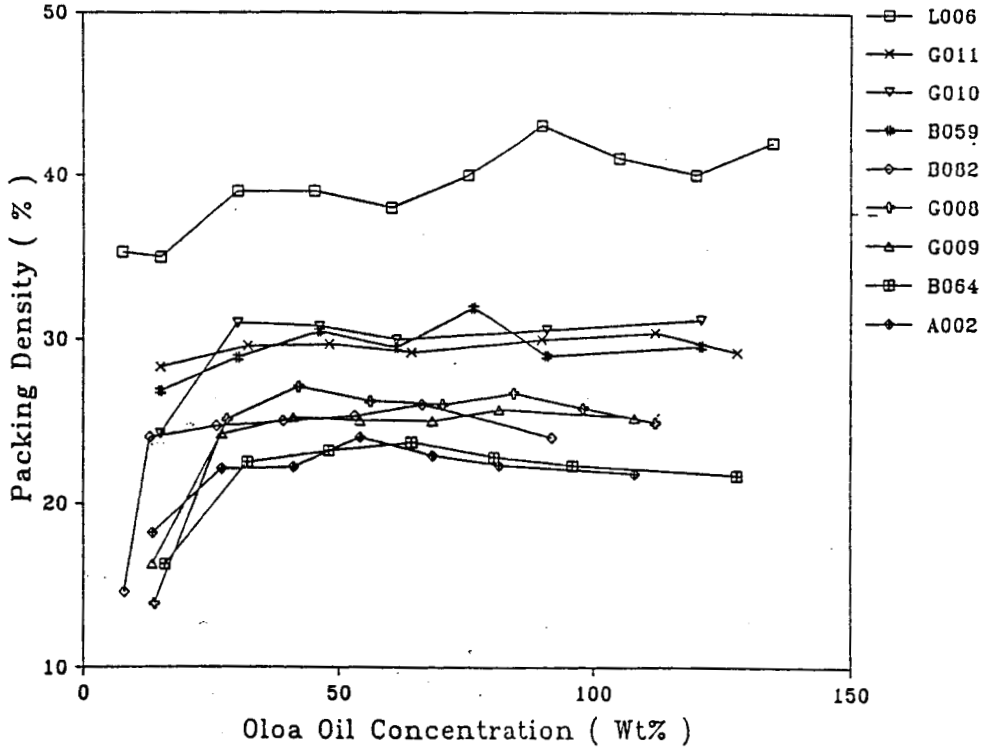

Figure 17. Centrifuged compact density as a function of Oloa concentration. Concentration of Oloa is based on powder weight. Centrifugal treatment is 3000 g's for 1 hr.

c. Packing Density and Dispersibility

Centrifuged compact densities exhibited different characteristic levels depending on powder type. A comparison of these density values with the previous dispersibility evaluation test results illustrates one important result. The low packing density of the B064 type powder is explained by its poor dispersibility. In poorly stabilized dispersions, particles coagulate quickly and the coagulated particles prevent the achievement of close packing due to geometrical restraints.

Good dispersibility does not insure good packing, as is illustrated by the difference between L006 and G011 type powders. In spite of similar dispersibilities, these two powders with their different particle size distributions showed quite different packing densities. Hence, additional factors must be taken into account to explain the experimental data.

d. Primary Agglomerate Size in the Oloa/Hexane System

Agglomerate size was measured for each powder immediately after a 5-minute ultrasonic treatment. The results are plotted against constituent BET particle diameters in Figure 18.

If the adsorption rate of Oloa molecules onto the surface of the SiC particles is much faster than the coagulation velocity, the agglomerate size will be close to individual particle size. Since the data show that the agglomerate sizes are 4-10 times larger than the constituent particle sizes, a limited amount of coagulation occurs prior to the formation of steric barriers which are good enough to prevent continued sticking of particles to one another. The agglomerated particles at the end of the fast coagulation period are the units from which compacts are formed. The characteristics of these primary agglomerates control compact properties.

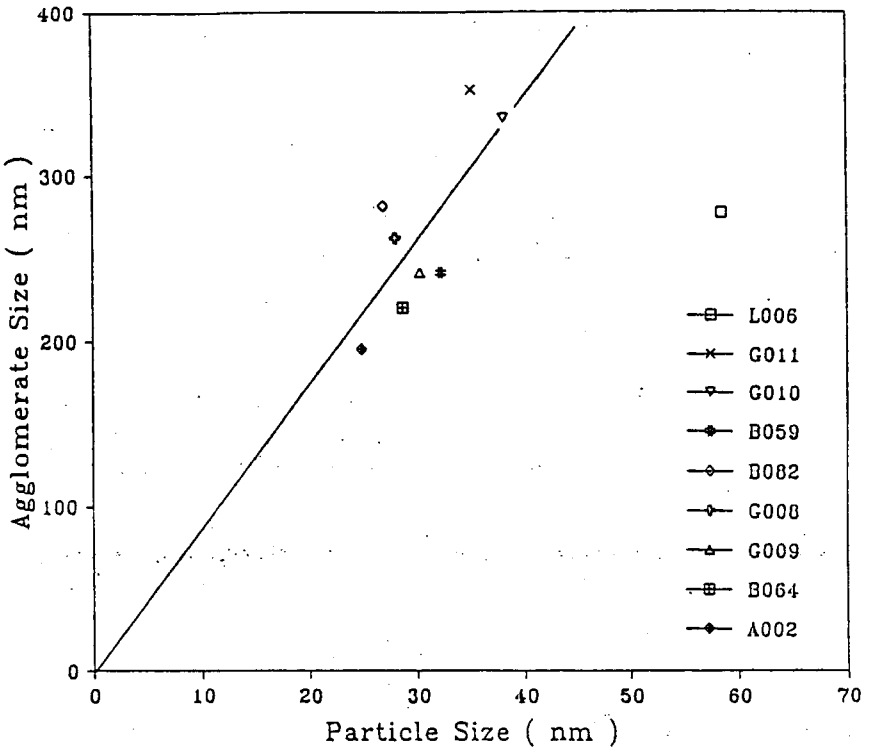

Figure 18. Primary agglomerate size as a function of the primary particle size (BET). Agglomerate diameters were measured immediately after ultrasonic treatment.

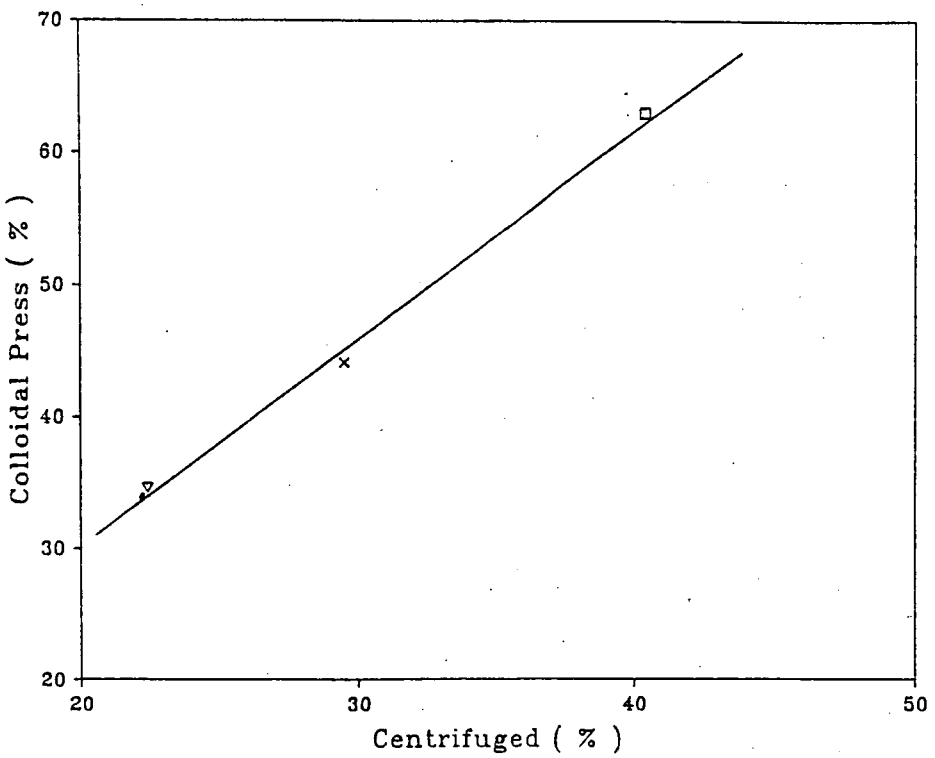

Figure 19. Comparison of the packing densities achieved in colloidally pressed green bodies and in centrifuged sediments.

e. Packing Density of Colloidally Pressed Parts

Colloidal pressing was performed with B064, G011 and L006 type powders applying a 69 MPa (10,000 psi) pressure. The results in Figure 19 show that the pressed densities were proportional to the centrifuged compact densities. This result indicates that the primary agglomerates which formed during the fast coagulation period and then became surrounded by Oloa-1200 are not breakable with this level of applied pressure range. Again, this illustrates the importance of making the primary agglomerate size as small as possible for enhancing the packing density.

The pressed densities achieved with L006 type powder deserve comment. At ~63% of theoretical, they reach the density of a random close-packed structure. This is the maximum density level that can be achieved with non ordered, uniform diameter spherical particles. Counting nearly touching neighbors, this structure has a coordination number slightly greater than 11.

Compacts were examined using SEM. The microstructures showed the importance of using small primary agglomerate size powders. The low density compacts (~33%) made with powder type B064 contained large pores. In contrast, the high density compacts (~63%) made with powder type L006 exhibited pore diameters approximately equal to the primary particle diameter.

3. Conclusions

Oloa-1200 in hexane was found to be an effective dispersant system for laser synthesized SiC. However, the specific powder is also important with respect to achieving small primary agglomerate sizes and maintaining them in a well dispersed state after stabilization by a steric layer.

The primary agglomerate size greatly affected the packing density. These primary agglomerates were not breakable with pressures up to 69 MPa (10,000 psi).

V. FORMATION OF SHAPES AND PARTS

The unique surface properties of these covalent materials, as well as the need to maintain high purity throughout processing, place unusual restrictions on the forming and shaping process as has been discussed. These restrictions include the choice of a non-contaminating dispersing medium and limited exposure to air and water vapor. In addition the choice as to whether or not to add additional components such as binders and lubricants specifically to aid post-dispersion forming is tempered by these restrictions as well as the restrictions imposed by drying and firing processes. Questions such as residue formation and effluent generation in a highly impermeable compact tend to discourage the use of binders and lubricants.[36] However, the proper selection of a dispersing system may perform these functions without incorporating additional compounds. H. Rumpf[37] has shown that liquid adhesion forces of low molecular weight compounds can improve green strength as well as increase the ability of a compact to plastically deform under stress. These characteristics enhance the ability of a wet compact to be consolidated by pressing and to maintain integrity after pressing. The choice of a forming technique was based on the desire to exploit these properties of fully wet compacts. The forming technique chosen was colloidal pressing.

A. Colloidal Pressing

The colloidal pressing process is analogous to the commercial practice

of slip filtration followed by wet pressing the filter cake. This process is capable of producing relatively defect free, high density compacts because colloidal pressing eliminates the possibility of incorporating macro-bubbles while loading the press with the filter cake. Colloidal pressing occcurs in two stages within one apparatus: filtration and consolidation.

1. Filtration

Filtration occurs initially as the solvent is forced through the porous membrane by the load on the piston. Particles build up on the membrane forming a filter cake. If the particles are perfectly dispersed and have a high interactional potential the individual particles will be added to the compact at a point of minimum potential (e.g. the saddle point of three particles). If the powder is monodispersed and the process occurs without long range ordering such a compact will have a maximum density of approximately 63% corresponding to random close packed structure.

In many systems however compact density falls short of this mark. Low density flocs containing voids may exist in the slip. A low interparticle interactional potential may allow the slip particles to add to the compact at the earliest interaction rather than adjusting to the minimum saddlepoint. Such behavior would result in a low density chainy structured compact. The force of the solvent flowing through a partially dense compact may subsequently result in channel formation.[38]

These mechanisms result from non-ideal dispersion characteristics and/or excessive filtration rates. These effects can be monitored by comparing the results of a simple filtration experiment with the theoretical model of fluid flow through a homogeneous powder compact as presented by Bird et al.[39]

$$V_o = \frac{\Delta P}{L+L'} \frac{D_p^2}{150\eta} \frac{\varepsilon^3}{(1-\varepsilon)^2}$$

where $V_o \equiv$ superficial fluid velocity

$\Delta P \equiv$ pressure differential across compact

$L \equiv$ instantaneous compact thickness

$L' \equiv$ effective bed thickness of filter

$D_p \equiv$ particle diameter

$\eta \equiv$ solvent viscosity

$\varepsilon \equiv$ void fraction

All quantities are directly measurable except L' which is calculated using the appropriate ε once the superficial fluid velocity (V_o) is measured for pure solvent passing through the membrane - filter assembly. The correlation between theoretical and experimental flow rates is a good means of monitoring the structure of the filter compact. An experimental flow rate less than the theoretical value is evidence of clogged interstitial passageways possibly resulting from a broad particle size distribution. If the experimental flow rate is greater than theoretical, a more highly permeable compact implies that low density, low resistance pathways are interspersed throughout the powder compact. These low resistance pathways are known as channels. These channels could later serve as critical flaws for fracture.

If the forming process ended here, as it would for slip casting or pressure filtration, the low density channelled structure would be retained and inferior parts would result. However the second phase of colloidal pressing serves to eliminate most of these potential flaw sites.

2. Consolidation

The consolidation stage of colloidal pressing begins when the opposing filtered compacts, that built up during filtration, impinge upon each other (for bidirectional flow) or the filtered compact impinges on the opposing non-porous plug (for unidirectional flow). During the normal procedure, the consolidation stage is accompanied by a rapid increase in the load at constant strain rate. During this process, the low density filter compact (typically 35% dense) undergoes substantial rearrangement. The average number of nearest neighbors increase from typically 6 to 11,[40] and channels that had formed during filtration collapse.

The consolidation process under constant rate of strain is treated in detail by Lambe and Whitman[41]. Some important issues that are discussed in this work are:

- pressure and density gradients go to zero as the strain rate goes to zero (assuming no die friction).
- as the load is removed the affinity that the compact has for the liquid can cause the fluid to be reabsorbed, resulting in compact swelling and possible fracture.
- the elasticity of the particles can also result in compact swelling during load release, serving as another mechanism toward compact fracture.

These three issues can be addressed individually by evaluating the integrity of the compacts (i.e. sintered strength under constant conditions) as a function of:

- strain rate
- rate of load removal
- limited maximum load

In addition, the issue of liquid reabsorption during load removal can be addressed by observing the effect of solvent removal from the compacts while under a load, followed by load removal.

B. Procedures and Results

1. Colloidal Pressing

Cylindrical pellets were formed by colloidal pressing using the die apparatus shown schematically in Figure 20. The solvent is extracted from the slip through membrane filters which cover porous stainless steel frits. The load is applied to the frits by ported stainless steel pistons, the die is brass. Two porous frits are used in bidirectional pressing and one is used for unidirectional pressing.

Silicon carbide and silicon slips were prepared by sonicating a 5 vol% solids-methanol mixture in a glass vial for three minutes at a power level of 65 watts. The slip was then pipeted into the die and pressed.

By visually comparing pellets that were colloidally pressed with unidirectional and bidirectional geometries, it was obvious that the latter geometry often resulted in laminate flaws in the middle of the compacts. These flaws were formed when the opposing filter cakes met. For this reason the bidirectional pressing geometry was abandoned. The results reported reflect the unidirectional flow geometry.

2. Filtration Stage

A baroid-type filter press obtained from Gelman Sciences, Inc. (#4280) was used in these experiments. A 5 volume % presonicated slip of SiC and 2-propanol was placed in the filter chamber fitted with a 0.22 μm teflon membrane (Millipore FG) filter. The chamber was closed and attached to a

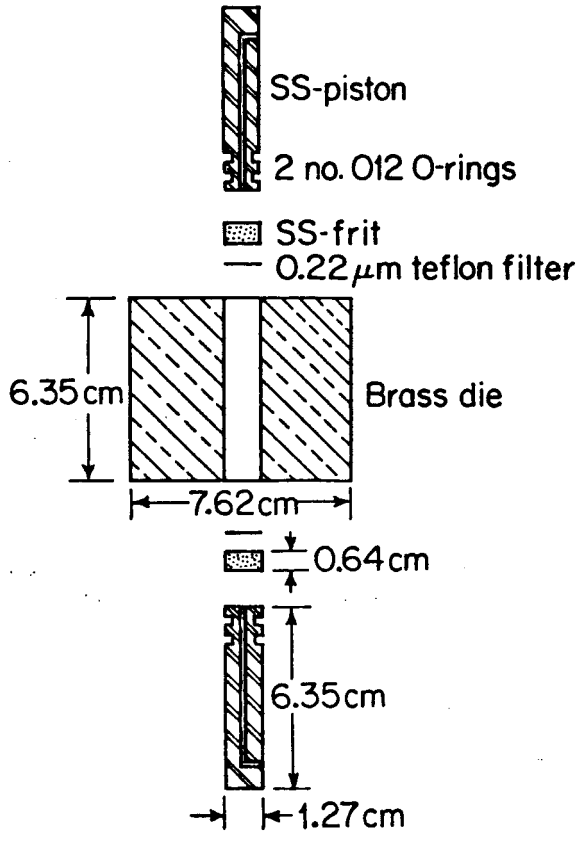

Figure 20. Components making up colloidal pressing apparatus.

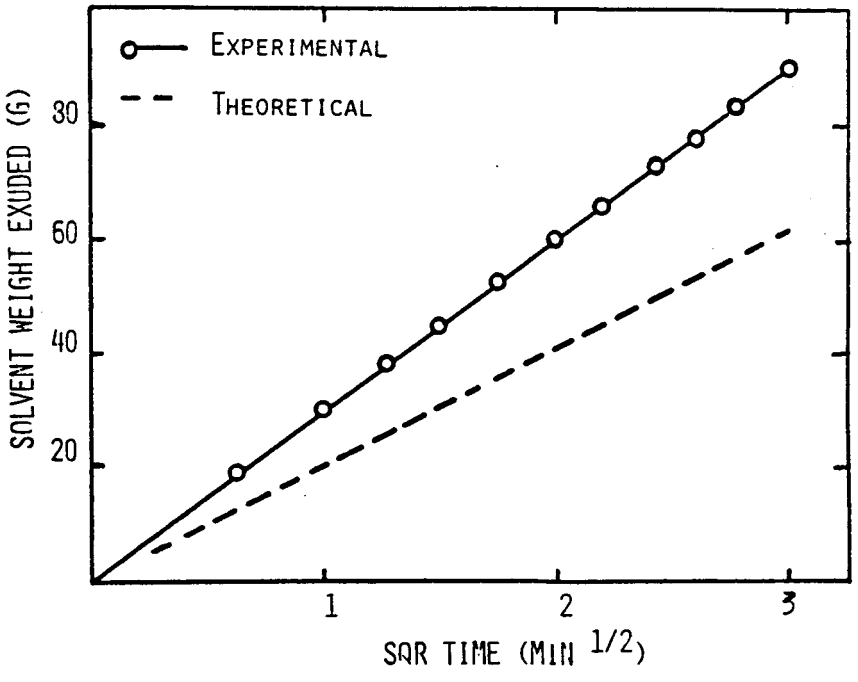

Figure 21. A comparison between solvent weight exuded and theoretically predicted values plotted against time to the one half for L-006 SiC powder at 5 vol % solids in 2-propanol under 0.06 MPa (10 psi) pressure.

regulated nitrogen pressure of 0.064 MPa (10 psi). At zero time, a toggle valve was opened exposing the chamber to the nitrogen pressure. Immediately clear fluid exuded from the lower chamber vent and poured into a tared beaker located on a Mettler AE-163 balance with RS-232 interface. A timer switch relayed the instantaneous weight of exuded fluid to a printer at five second intervals. When the fluid stopped, the experiment was halted and the volume of the cake was determined by bulk measurements. The weight was determined after drying in nitrogen for 24 hours at 180°C.

The weight of solvent exuded from the baroid press is plotted in Figure 21 as a function of time to the one half power. The initial flow rate is used to calculate the effective thickness of the filter (L') and the compact void volume is determined by bulk measurements of the cake. These parameters are used to calculate the theoretical weight of solvent as a function of time to the one half power which are also plotted in Figure 21.

The theoretical and experimental data are straight lines as expected. The discrepency between the two slopes indicates that the actual cake is more highly permeable than the theoretically homogeneous structure assumed in the model, strongly suggesting that channels were formed under these experimental conditions as were observed by Aksay[38] in slip cast samples.

3. Consolidation Stage

Using the colloid press the filtration stage occurs at very low pressures, typically <0.64 MPa (<100 psi). The solvent is exuded from the piston port at a rate of $1cm^3/cm^2$ of filter/minute. Compact densification due strictly to filtration is typically 30-40%. Once the slip has been filtered and the opposing compacts impinge in the case of bidirectional pressing or the compact impinges on the non-porous plug in the case of

unidirectional pressing, the pressure increases as the strain rate is maintained. This occurs in less than one minute during which time the compact density increases to a maximum value of 63%. During this consolidation stage approximately 0.2cm^3 of solvent is extruded. The pressure is held at a maximum while stress gradients are allowed to relax for 1/2 to 60 minutes. Remaining residual stress gradients are due to the piston-die and compact-die friction. The former is minimal due to the low coefficient of friction of silicone lubricated viton O-rings on the brass barrel; the latter is also small due to the low aspect ratio of the pellet geometry (i.e. thickness : diameter <1:5). A homogeneously dense microstructure should result in the absence of stress gradients, and the channels that formed during filtration should be eradicated by this consolidation rearrangement.

The effects of maximum loads on pellet densities are given in Figure 22 for silicon compacts. The density rises with increased maximum load as predicted.[42-44] According to Bashin[43] the relationship between density (ρ) and pressure (P) is given by:

$$\rho = \frac{k}{\log P} + c$$

where k and c are constants.

The derivation of this equation is based on the assumption that the energy inputed into the system is equivalent to $P \cdot \Delta V$ and that the incremental work done on the cake is related to the log of the incremented density change. It is expected that this relationship should hold true up to the point of fully dense compaction (i.e. particle to particle contact) or up to the onset of particle fracture.

Data for thirty colloidally pressed silicon powder compacts (B-004-SED) is given in Figure 22 over a wide range of colloidal pressing pressures.

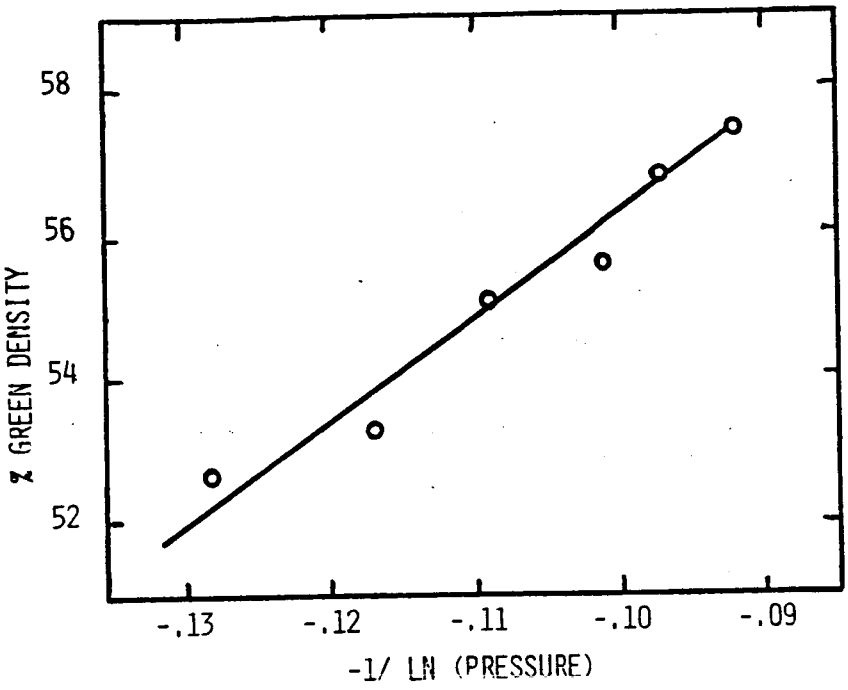

Figure 22. Green compact density as a function of negative inverse log maximum colloidal pressing pressure for B-004-SED Si and SiC powders in methanol.

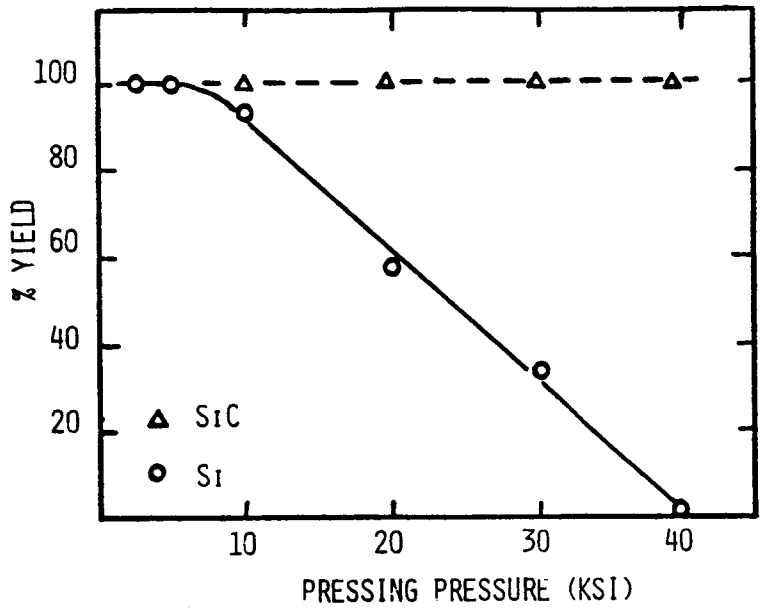

Figure 23. Percent yield of good green compacts versus maximum colloidal pressing pressure for B-004-SED Si powder in methanol.

The close fit implies that a single process governs compaction and that particulate fracture is not occurring.

The green compact integrity is reflected in Figure 23 as % yield during pressing versus maximum load. The yield for the silicon compacts drops dramatically above 69 MPa (10,000 psi) while the yield remains constant for SiC. We do not have an explanation for this difference between the two materials.

Green silicon compact density is plotted as a function of time in Figure 24. For times longer than one half minute density is constant. This implies that the stress relaxation is very short for laser synthesized silicon compacts. The same behavior is expected for laser synthesized silicon carbide powder.

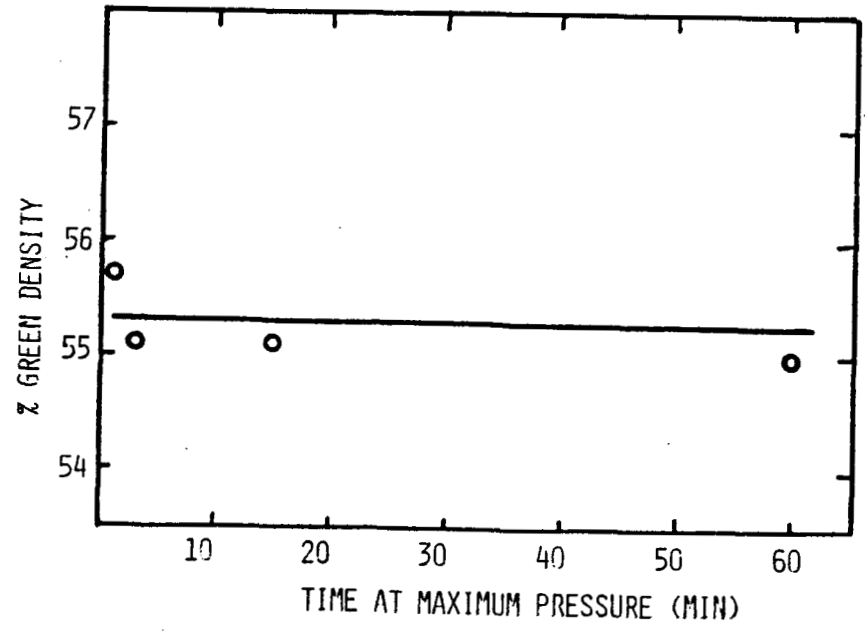

Figure 24. Green silicon compact density versus time at maximum colloidal pressing pressure.

C. Summary

The densities of the compacts have increased continuously during the program as powder synthesis techniques, dispersion techniques and pressing techniques have been developed. A major contribution to increased compact density has been the improved powder characteristics. Controlling aggregation and particle size distribution is important for achieving the more dense compacts. Laser synthesized SiC compact densities up to 63% have been achieved.

This density (63%) corresponds approximately to the theoretical value for uniform spheres in a random close packed structure, which has the maximum possible achievable density without introducing ordering. Including "nearly touching" neighbors, this structure has a coordination number in excess of 11 thus approaching that of close packed arrays in its perfection.

VI. DENSIFICATION

Less than planned levels of effort were actually spent on the densification studies. Initial shaping study results indicated that green densities were too low to yield useful final microstructures. Starting from green densities as low as ~ 40%, we anticipated large residual pores, discontinuous grain growth and unacceptably low final densities. Only after recent synthesis procedures produced the improved powders from which green densities in excess of 60% could be achieved, was it reasonable to undertake densification research.

This research should be viewed as an initial demonstration of densification feasibility, the definition of necessary time-temperature combinations, and a preliminary evaluation of the resulting parts. We have determined the resulting density after a one hour sintering cycle at temperatures ranging from 1800 to 2100°C. The single powder type used for these experimentes was selected on the basis of maximum green densities. Resulting parts were characterized with respect to density, microstructure, phases, strength, hardness, and fracture toughness.

A. Experimental Procedures

1. SiC Powder

Silicon carbide powder type L-033 was used for these initial densification studies. The corresponding undoped powder synthesized under the same process conditions exhibited the highest, reproducible green density parts made by colloidal pressing. Introduction of approximately 1% by weight of B into the reactant gas stream as B_2H_6 caused no noticible changes in any powder or green pellet characteristics. This powder has a mean diameter of 0.1 μm and a standard deviation of ~ 20% on a weight basis. The nominal composition was 3% excess carbon by weight. As synthesized, this powder is 100% β SiC.

2. Pellet Pressing

Nominally 1 cm diameter by 2 mm thick green pellets were made by colloidal pressing. Powders were dispersed in octyl alcohol at a concentration 400 mg powder in 3.5 ml of liquid using a 60 watt ultrasonic probe for 5 minutes. This system was selected on the basis of the pure

solvent dispersion study. Dispersants were avoided since we could not rule out possible adverse effects of adsorbed molecules. Pellets were pressed with unidirectional flow for 15 minutes at a die pressure of 13.7 MPa (2000 psi). These procedures yielded green pellets having densities of 62-64%; the range represents the measurement error.

3. Drying

After pressing, the pellects were dried to remove all volitiles to avoid damaging the parts during firing. Drying was accomplished with a 24 hour soak in a 200°C N_2 atmosphere after an 8 hour linear ramp. The completeness of this drying cycle was established by weight loss measurements as a function of exposure time.

4. Firing

Dried samples were fired at temperatures ranging from 1800 to 2100°C in a graphite tube furnace. The samples were supported vertically in a slotted carbon channel with a nominally 3 mm spacing between samples. The Ar atmosphere was established with a 2 hour flush before heating was initiated. The heating cycle consisted of a 50°C/hour linear ramp to the firing temperature, a one hour soak and a furnace quench (50-100°C/hour).

5. Exposures

The powders and pellets were handled without air exposure until the pressed green pellets were seperated from the Teflon™ filters. This step was done in air because it is impossible to avoid damage using the glove box gloves. The pellets were exposed to air again when, after drying, they were transported from the glove box to the firing furnace.

B. Results

1. Physical and Microstructural Features

Samples were characterized with respect to density using three techniques and in terms of phase content by X-ray diffraction. Densities were determined by physical dimensions and weight, by immersion in water, and by microstructural analysis using SEM and optical microscopy of both fractured and polished surfaces. The results are shown in Table 8.

For temperatures up to 2050°C, densities increased with incresing maximum sintering temperature. The average density of the 2100°C sample exhibited an apparant decrease; however, we suspect the accuracy of two of the density determinations. The bulk measurements (immersion and dimensional) included porous regions near the samples' surfaces thus the apparent densities were probably lower than the true values. Also, the polished 2100°C sample contained many pull-outs which were counted as pores, thus the apparent density was lower than true. Pore diameters also exhibited an initial decrease in diameter followed by an apparent increase. In part this increase is the result of counting the pull-outs as pores.

When plotted as an Arrhenius function, the linear shrinkage shown in Figure 25 exhibits an apparent activation energy of ~120 kcal/mole. This value nominally corresponds to the activation energy reported for carbon diffusion through SiC grain boundaries.[45] No detailed mechanistic studies were conducted; however, the inferred rate controlling mechanism appears reasonable.

The sintered SiC remained 100% β phase up to a sintering temperature of 2050°C. The 2100°C sample contained approximately equal fractions of α and β phases. These results show that the sintered material has adequate phase stability for most applications considered appropriate for SiC.

Table 8. Characteristics of Sintered SiC

	Sintering Temperature (°C)					
	1800	1900	1950	2000	2050	2100
Density (%)						
Dimensional	67.2	72.3	85.5	91.3	103.3	81.4
Immersion	64.4	82.6	86.3	93.3	96.3	87.8
Microstructural						
Fracture Surface	<70.0	--	--	>95.0	--	~100
Polished Surface	--	88.2	95.7	--	96.1	91.4
Average	65.8	81.0	89.1	93.2	97.5	90.2
Pore Diameter (Å)	--	90	37	--	530	735
Grain Shape	--	equiaxed	equiaxed and elongated	--	elongated	equiaxed
Grain Size (μm)		0.3	0.25 and 0.5 X 2.0	--	1.2 X 20	100
Phase	--	β	β	β	β	α + β
Tensile Strength (MPa)	--	--	--	--	645 ± 60	--
Vickers Hardenss (kg/mm^2)	--	--	--	--	2430 ± 313	--

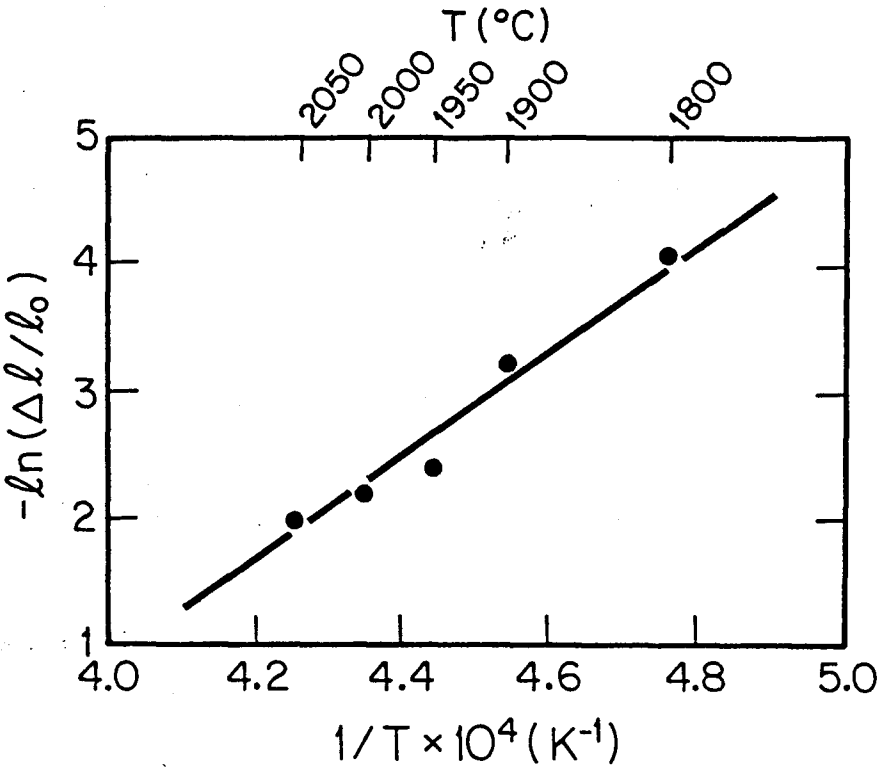

Figure 25. Arrhenius plot of fractional densification versus absolute temperature observed for B doped laser synthesized SiC. The activation energy is approximately 120 kcal/mole.

The grain size and morphology changed continuously with increasing firing temperature. At the lowest temperature examined (1900°C), the average grain size had already increased to approximately 0.3 μm from the starting dimension of ~0.1 μm. This dimension may be somewhat higher than actual because it was difficult to resolve individual grain boundaries within ~0.6 μm clusters which were counted as individual grains. Many 0.1-0.15 μm grains were observed in the 1900°C sample. By 1950°C, there was considerable coalescence of the particles into elongated grains similar to those reported by Sato et al[46] (Figure 26). They attributed this preferential growth of β SiC grains to a coincidental alignment of crystalline lattices between adjacent grains. Individual, small diameter, equiaxial grains still remain after firing at 1950°C. With 2050°C firing, the microstructure appears to be made up completely of high aspect-ratio

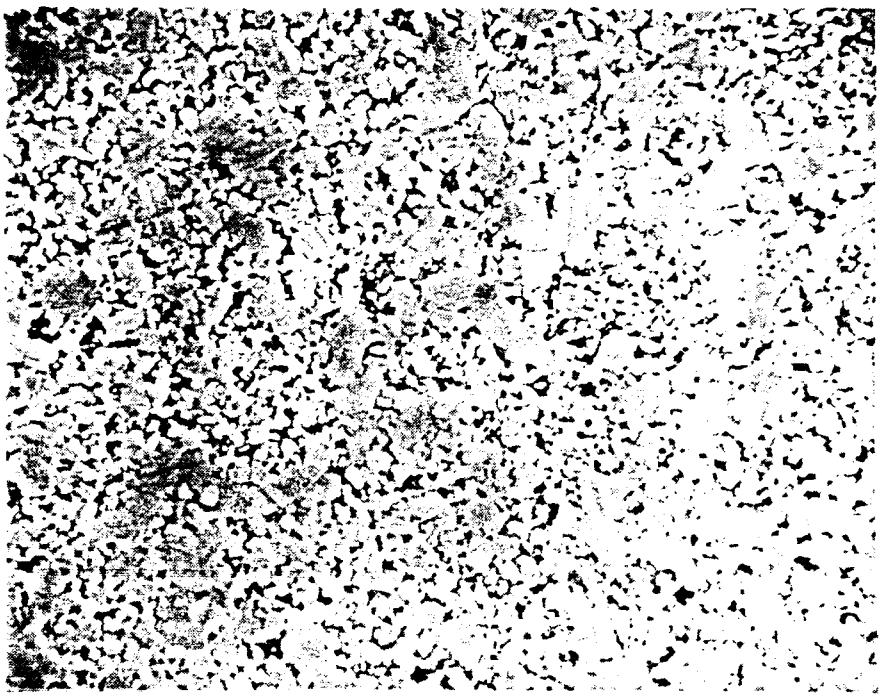

Figure 26. SEM of B doped SiC sample sintered at 1950°C for 1 hr in Ar. Magnification 9200X.

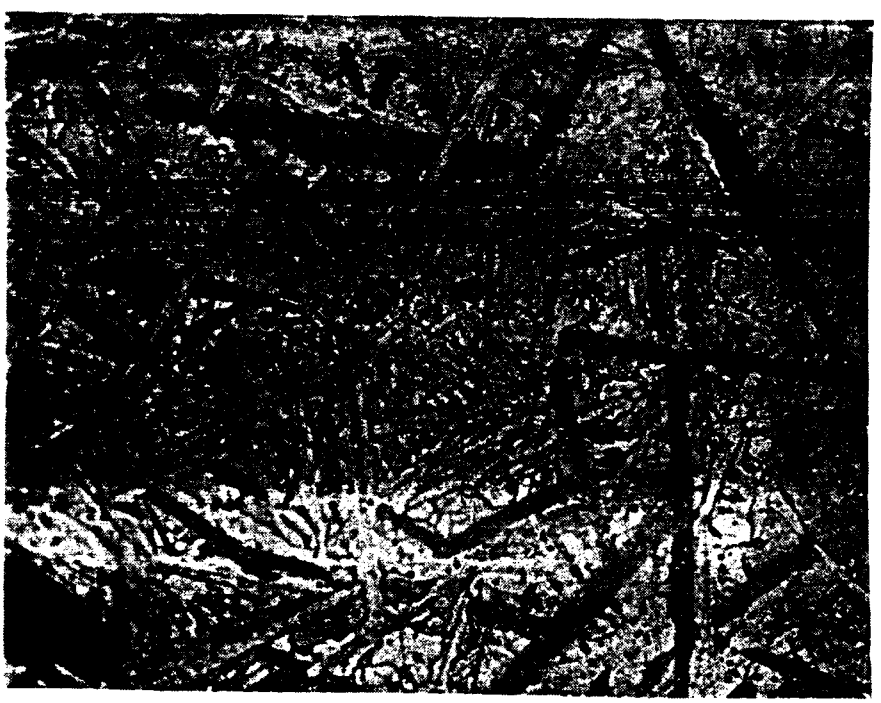

Figure 27. Optical photomicrograph of B doped SiC sample sintered at 2050°C for 1 hr in Ar. Magnification 1000X.

cylindrical β grains approximately 1.2 μm in diameter and 20 μm long (Figure 27). Pores are confined to grain boundaries. With partial conversion to α SiC at 2100°C, equiaxed grains grow to 100 μm; pores are uniformly distributed throughout the grains.

It is evident that considerable mass-transport occurred in the 1900-1950°C temperature range. We believe that higher, more uniform coordination numbers made possible with improved dispersion and pressing techniques should permit sintering temperatures to be reduced to this temperature range. The grain growth mechanisms must be suppressed to permit service temperatures above ~2050°C.

2. Mechanical Properties

Room temperature strengths, hardness and fracture toughness characterizations were made for the 2050°C samples. Strengths were measured in biaxial tension using the ball-on-ring procedure. Hardness and fracture toughness were measured using a Vickers indentor.

The ball-on-ring test was used to eliminate spurious edge effects. An apparatus based on the design by Wachtman et al[47] was used in conjunction with an Instron Corp. universal testing machine. The ball diameter was 6.35 mm. The samples were tested using a fast crosshead speed (0.05 cm/min). Fracture strength, σ_f, was calculated [48] from:

$$\sigma_f = \frac{3P(1+\nu)}{4\pi t^2}\left[1+2\ln\frac{a}{b}+\frac{(1-\nu)}{(1+\nu)}\left(1-\frac{b^2}{2a^2}\right)\left(\frac{a^2}{R^2}\right)\right],$$

where P = fracture load, ν = Poisson's ratio (taken to be 0.25), t = sample thickness = 1 mm, R = sample radius = 6.35 mm, a = load support ring radius = 6.27 mm and b = ball contact radius (taken to be 0.333 mm = t/3).

The results of the strength measurements with the 2050°C SiC samples are included in Table 8. Although the samples are far from optimal, the observed average strength (645 MPa, 93,500 psi) is approximately 2 times strengths normally observed for sintered silicon carbide[49] and are more typical of hot pressed or HIPed SiC. The improved strength values probably result from the uniformly distributed, small diameter pores made possible with these ideal SiC powders and the post-synthesis processing procedures that were developed. Further optimization of the firing schedule can be expected to result in higher densities, smaller pores and less grain growth; all of these should result in further improvements in intrinsic strength levels. It should be noted that surface finish and related machining flaws can be expected to dominate observed strengths at this strength level if finishing operations are not done with great care as was observed with laser synthesized reaction bonded silicon nitride.[50]

Vickers hardness values were determined on polished surfaces using 300 and 500 gram loads. The observed values of 2430 kg mm^{-2} are also more typical of hot pressed rather than sintered SiC. We presume that the hardness and strength values are coupled, although there is no formal theory to relate the two properties in a brittle material as exists for ductile materials.

Fracture toughness values could not be measured on this material using the indentation technique. Normally with increasing loads, stable cracks originate from the corners of indention; the crack dimensions are used to calculate the K_{IC} values. Stable cracks did not form in this SiC material. Suddenly with increasing load, cracks formed and propagated completely through the samples. Similar results have been observed with other fine grain size SiC.[51,52]

VII. SUMMARY AND CONCLUSIONS

This research program has focused on the processing-microstructure-property paradigm first proposed by MIT. Only through the use of both highly perfect powders and careful post-synthesis processing steps will it be possible to achieve uniform, defect-free microstructures and the property improvements that are critical for many high performance applications. Specific issues addressed in this program have been the synthesis of SiC powders, their dispersion, their shaping into high quality green parts, consolidation of the green parts into dense bodies, and the evaluation of resulting properties.

Powder synthesis research began from successful demonstration of the feasibility of making SiC powders from laser heated SiH_4 and either C_2H_4 or CH_4 gases. The principal technical objective was to increase paricle diameters from 100-300 Å to nominally 1000 Å while retaining the other required characteristics (uniform particle size, freedom from agglomerates, purity and shape). In the course of this reserch, we found that the nucleation and growth model we had used to describe the process did not in fact apply; rather, particles formed by a two step reaction that involved collision and coalescence of molten silicon particles prior to the onset of the carburization reaction. With this understanding, it was possible to increase the particle diameter to the desired range. Controlling this type of reaction requires a precise combination of exposure times, temperature gradients and reactants. Fortunately, these are achieved in a straightforward manner with the laser heated gas phase powder synthesis process.

New dispersion techniques were required for these laser synthesized SiC powders because their surfaces are fundamentally different from all SiC powders that have experienced an exposure to air or water. Anerobic, anhydrous processing conditions were used throughout. Both pure solvent and sterric stablized dispersion techniques were investigated. It was felt that the pure solvent systems would be easier to dry and would leave less residue than the steric systems, but they probably would not be capable of achieving highly stable, high density dispersions.

Suitable pure solvent (oleic acid) and steric stabilized systems (Oloa/hexane) systems were identified for the high purity, laser synthesized powders. Considerable variation in the packing densities was observed between parts made from different powder lots having similar physical and chemical characteristics. It is believed that these differences result from varying degrees of agglomeration.

Green parts were made by centrifugal sedimentation and by colloidal pressing. Both techniques produced uniform parts that were free of large defects. The colloidal pressing technique yielded higher densities. Two stages of pressing were modeled: liquid is first extruded through a progressively thicker cake, then higher densities are made possible with particle rearrangement accompanying increasing pressure. Densities corresponding to a random close packed structure (~63.5%) were achieved; this is the highest possible density for non-ordered, uniform-diameter spheres.

After drying, the parts were densified for 1 hour at temperatures ranging form 1800 to 2100°C. Densities increased progressively with temperature up to 97.5% at 2050°C. The lower density exhibited by the 2100°C sample may be real because of pore entrapment behind grain boundaries

or may be artificial due to pull-outs and other measurement errors. Grain sizes increased with firing temperatures. Judging by the observed grain growth, the optimum firing temperature will probably be substantially below 2050°C.

Even without optimization, the properties of the resulting parts were excellent. Densities were high (up to 97.5%) and residual porosity was generally distributed uniformly throughout the parts in small diameter pores. The grain size and shape changed substantially during the evolution of the microstructures; β grains became progressively elongated and larger with increasing firing temperatures up to 2050°C. At 2100°C, they transformed to much larger equiaxial α and β grains with entrapped pores.

The biaxial tensile strengths of the 2050°C parts were also excellent. The strengths (up to 714 MPa, 103,500 psi) are twice levels nominally observed for sintered SiC and are more typical of hot pressed SiC. Hardness values (2430 kg/mm^2) were also more typical of hot pressed than sintered SiC. Both result from the absence of large defects and the confinement of residual porosity to small diameter, uniformly distributed pores. Fracture toughness values could not be measured by the indentation technique because stable cracks did not form; when cracks were induced they propagated to the samples' boundaries.

This research program accomplished all of its major objectives. Broadly, the overall goal was to demonstrate that superior microstructures and properties could be achieved by using both powders having ideal characteristics and very specific post-synthesis processing procedures. This was accomplished. In achieving this objective, several narrower technical issues were resolved. These included finding means to make the powders, disperse the powders, shape the powders into high-density flaw-free

parts, dry the parts and densify the parts. While superior properties and both reduced densification times and temperatures were demonstrated, these results do not represent fully optimized process conditions or maximum property values. Further improvements can be anticipated.

VIII. REFERENCES

1. Report of the Panel on High Temperature Ceramics, U. S. Department of Energy, Materials Science Program, January 1979.

2. Haggerty, J. S., Flint, J.H., Garvey, G. J., Lihrmann, J-M. and Ritter, J. E., "High Strength, Oxidation Resistant Reaction-Bonded Silicon Nitride From Laser-Synthesized Silicon Powder", Proceedings 2nd International Symposium, Ceramic Materials and Components for Engineers, Lübeck-Travenmünde, Federal Republic of Germany, April 1986.

3. Bernal, D. and Mason J., Nature, 188, 908 (1960).

4. Haggerty, J. S., and Cannon, W. R., October 1978, Sinterable Powders from Laser Driven Reactions, under Contract N00014-77-C0581, M.I.T., Cambridge, MA.

5. Haggerty, J. S., and Cannon, W. R., July 1979, Sinterable Powders from Laser Driven Reactions, under Contract N00014-77-C0581, M.I.T., Cambridge, MA.

6. Haggerty, J. S., and Cannon, W. R., July 1980, Sinterable Powders from Laser Driven Reactions, under Contract N00014-77-C0581, M.I.T., Cambridge, MA.

7. Haggerty, J. S., July 1981, Sinterable Powders from Laser Driven Reactions, under Contract N00014-77-C0581, M.I.T., Cambridge, MA.

8. Suyama, Y., Marra, R.M., Haggerty, J. S., and Bowen, H. K., Am. Cer. Cer. Soc. Bul. 64[10], 1356 (1985).

9. Mizuta, S., Cannon, W. R., Bleier, A. and Haggerty, J. S., Am. Ceram. Soc. Bul., 61, 872 (1982).

10. Marra, R.A., "Homogeneous Nucleation and Growth of Silicon Powder from Laser Heated Gas Phase Reactants", Ph.D. Thesis, MIT, Cambridge, MA 1983.

11. Sawano, K., "Formation of Silicon Carbide Powder from Laser Induced Vapor Phase Reactions", Ph.D. Thesis, MIT, Cambridge, MA 1985.

12. Flint, J.H., Garvey, G., Lightfoot, A., Harris, C. and Haggerty, J.S., "Improved Laser Synthesized Ceramic Powder", presented 88th Annual Meeting The American Ceramic Society, Chicago, IL, May 1986, Paper No. 19-BP-86.

13. Smoluchowski, M.V., Z. Physik. Chem. (Leipzig), 92, 9 (1917).

14. Lee, K.W., Colloid Interface Science, 92, 315 (1983).

15. Lee, K.W., Chen, H., and Gieseke, J.A., Aerosol Sci. and Tech. 3, 5362 (1984).

16. Skinner, G.B. and Sokoloski, E.M., J. Phys. Chem., 46, 1028 (1960).

17. Chen, C.T., Back, M.H., and Back, R.A., Can. J. Chem., 53, 3580 (1975).

18. Coltrin, M.E., Kee, R.J. and Miller, J.A., J. Electrochem Soc., 131[2], 425 (1984).

19. Govila, R.V., J. Mat. Sci., 19, 2111-2126 (1984).

20. Dutta, S., J. Mat. Sci., 19, 1307-1313 (1984).

21. Hamminger, R., Grailwahl, G., Thummler, F., J. Mat. Sci. 18, 353-354 (1983).

22. Hermansson, L., Carlstrom, E., Persson, M. and Carlsson, R., Proc. of International Symposium on Ceramic Components for Engines, 1983 Japan.

23. Bowen, H.K., "Physics and Chemistry of Packing Fine Ceramic Powders", MIT Report, 1980.

24. Barringer, E.A., "The Synthesis, Interfacial Electrochemistry, Ordering and Sintering of Monodispersed TiO_2 Powders", Ph.D. Thesis, MIT, Cambridge, MA, 1983.

25. Schilichting, J., "Transport Mechanism Through Oxide Surface Layers on Silicon Ceramics", Institute Chem. Technik of Karlsruhe University, Karlsruhe, W. Germany, 1980.

26. Carlstrom, E., Tijernlund, A.K., Hermansson, L. and Carlsson, R., "Influence of Powder and Green Compact Characteristics on Microstructure of Sintered Alpha SiC", Swedish Institute for Silicate Research, Gothenburg, Sweden, 1982.

27. Paifitt, G.D., "Fundamental Aspects of Dispersions", in Dispersions of Powders in Liquids, (G.D. Parfitt, ed.) Englewood: Applied Science Pub., 1981.

28. Bleier, A., J. Amer. Cer. Soc., 66, C-79 (1983).

29. Mizuta, S., Cannon, W.R., Bleier, A., and Haggerty, J.S., Am. Cer. Soc. Bull., 61, 872-875 (1982).

30. Sollner, K., J. Phys. Chem., 42[8], 1071 (1938).

31. Aoki, M., Ring, T.A., and Haggerty, J.S., "Analysis and Modeling of the Ultrasonic Dispersion Technique", presented 88th Annual Meeting The American Ceramic Society, Chicago, IL, May 1986, Paper No. 61-BP-86.

32. Verwey, E.J.W. and Overbeek, J.T.N.G., The Theory of Stability of Lyophobic Colloids, Elsevier Press, Amsterdam, 1948.

33. Napper, D.H., Polymeric Stabilization of Colloidal Dispersions, Academic Press, NY, 1983.

34. Okuyama, M., Garvey, G., Ring, T.A., and Haggerty, J.S., "Dispersion of Laser Synthesized Silicon Carbide in Non-Aqueous Solvents", presented 88th Annual Meeting The American Ceramic Society Chicago, IL May 1986, Paper No. 63-BP-86.

35. Aoki, M., Garvey, G., Ring, T.A., and Haggerty, J.S., "Dispersion and Compaction Behavior of Laser Synthesized Silicon Carbide", presented 88th Annual Meeting The American Ceramic Society, Chicago, IL, May 1986, Paper No. 60-BP-86.

36. Castro, D., Ring, T.A., and Haggerty, J.S. "Drying High Density Laser Synthesized Silicon Compacts", presented 88th Annual Meeting The American Ceramic Society, Chicago, IL, May 1986, Paper NO. 62-BP-86.

37. Rumpf, H. and Schubert, H. in Ceramic Processing Before Firing, ed. G.Y. Onoda and L. Hench, J. Wiley and Sons, NY (1978).

38. Kim, S.I., and Aksay, I.A., Aksay, Amer. Cer. Soc. Bull. Abstracts (102-B-84P), June 1984.

39. Bird, R.B., Steward, W.E. and Lightfoot, E.N., Transport Phenomena, J. Wiley and Sons, NY (1960).

40. Rhines, F.N. in Ceramic Processing Before Firing, G.Y. Onoda and L.L. Hench, J. Wiley and Sons, NY (1978).

41. Lambe, T.W. and Whitman, R.V., Soil Mechanics, J. Wiley, NY (1969).

42. Walker, E.E., Trans. Faraday. Soc., 19, 73 (1923).

43. Bashin, M.Y., Vestnik Metalloprom, 18[2], 124-127 (1938).

44. Heckel, R.W., AIME Trans, 221[5], 1001-1008 (1961).

45. Thümler, F., in Sintering Processes, G. C. Kuczynski (ed.), Plenum Press, NY (1980)

46. Sato, H. Otsuka, N., Liedl, G.L. and Mansour, S., Mat. Lett., 4[3], 136 (1986).

47. Wachtman Jr., J.B., Capps, W. and Mandel, J., J. Mat. Sci., 7[2], 188 (1972).

48. Shelty, D.K., Rosenfield, A.R., McGride, P., Bansal, G.K. and Duckworth, W.H., Am. Cer. Soc. Bull., 59[12], 1193 (1980).

49. Dutta, S., J. Am. Cer. Soc., 68[10], C-269 (1985).

50. Haggerty, J.S., Garvey, G., Lihrmann, J-M. and Ritter J.E., "Processing and Properties of Reaction Bonded Silicon Nitride Made From Laser Synthesized Silicon Powders", Proc. of Materials Research Soc. Symposium (L) Defect Properties and Processing of High-Technology Nonmetallic Materials, 12/2-4/85, Boston, MA.

51. Ritter, J.E., Univeristy of Massachusetts, private communication.

52. Mehra, R., "The Effect of Erosion on Material Removal and Strength Degradation of α-SiC", M.S. Thesis, University of Massachusetts, Amherst, MA 1985.